Synthesis of Oxide Based Ceramic Thin Films for Methanol Electro-Oxidation in Direct Methanol Fuel Cells

Rimsha Liaqat

Regn. No: 00000278228

This work is submitted as a MS thesis in partial fulfillment of the requirement for the degree of

(MS in Chemistry)

Supervisor's Name

Dr. Muhammad Adil Mansoor

Department of Chemistry

School of Natural Sciences (SNS)

National University of Sciences and Technology (NUST), H-12

Islamabad, Pakistan

2021

FORM TH-4

National University of Sciences & Technology

MS THESIS WORK

We hereby recommend that the dissertation prepared under our supervision by: Rimsha Liaqat, Regn No. 00000278228 Titled: Synthesis of Oxide Based Ceramic Thin Films for Methanol Electro-Oxidation in Direct Methanol Fuel Cells be Accepted in partial fulfillment of the requirements for the award of **MS** degree.

Examination Committee Members

1. Name: Prof. Muhammad Mazhar Signature: _____

2. Name: Dr. Manzar Sohail Signature: _____

External Examiner: Dr. Rabia Naeem Signature _____

Supervisor's Name Dr. M. Adil Mansoor Signature: _____

_____ 20/1/21
Head of Department Date

COUNTERSINGED

Date: 20/1/2021

Dean/Principal


بسم الله الرحمن الرحيم

Dedication

This study is wholeheartedly dedicated to my beloved parents, who have been always my source of strength.
To my supervisor who always shared his words of guidance, advice and encouragement.

Acknowledgements

All praises to **Allah Almighty** for blessing me with intellect, courage and stamina to complete my research work. Nothing would have been possible without His grace. Trembling lips and wet eyes praise for **Holy Prophet Hazrat Muhammad (PBUH)** for enlightening my conscience with the essence of faith in Allah.

I pay my deepest gratitude to my supervisor **Dr. Muhammad Adil Mansoor** for his guidance, valuable cooperation for my research work, spiritual and moral support throughout the research journey. He played pivotal role in accomplishment of this project. He always managed to guide me in the right research direction and never cared about working hours. I am really thankful to him.

I pay my cordial thanks to my GEC members **Prof. Dr. Muhammad Mazhar** and **Dr. Manzar Sohail** for their assistance, kindness and guidance.

I am thankful to HoD chemistry **Dr. Muhammad Arfan** to ensure the availability of positive research environment. I would also like to acknowledge all the faculty and lab staff of SNS for being so cooperative and kind.

I am thankful to School of Natural Sciences (SNS) for financial support and US Pakistan Center of Advanced Studies in Energy (USPCAS-E) for facilitating me in characterization of my materials.

I am grateful to Allah for blessing me with a family who has backed me and has given me courage, love, and support that I needed. I am thankful to my ideal my father **Liaqat Ali**, my beloved mother and brothers (**Ahsan Ali, Mohsan Ali**).

I also want to acknowledge my research fellows and friends especially **Farah Ahmad and Maria Ashraf** for their support and loving memories.

Last but not the least, I want to acknowledge myself for all the hardships through which I have successfully made this journey.

Rimsha Liaqat

Abstract

Methanol electrochemical oxidation in direct methanol fuel cell (DMFC) is considered as an efficient pathway for generating renewable energy with low pollutant emissions. In this work, NiO, CuO, Cr_2O_3, NiO-CuO and $Ni_{1-x}Cr_xO_2$ thin films were synthesized by a simple dip-coating method and tested for electro-oxidation of methanol. These synthesized electrocatalysts were characterized by X-ray diffraction spectroscopy (XRD), Scanning electron microscopy (SEM), Energy-dispersive X-ray spectroscopy (EDS), and Raman spectroscopy. The electro-catalytic activity for methanol oxidation was studied by different techniques such as linear sweep voltammetry (LSV), electrochemical impedance spectroscopy (EIS), and chronoamperometry (CA). In the presence of 0.3 M methanol, the current densities of NiO-CuO and $Ni_{1-x}Cr_xO_2$ thin films are 6.1 mA0.5cm^{-2} and 6.5 $mAcm^{-2}$ vs. 0.6 V. The increase in the catalytic activity of NiO-CuO and $Ni_{1-x}Cr_xO_2$ thin films can be due to a synergistic effect between metal oxides. The findings of EIS and CA also support the above results and help to explain the assumptions described. All the results of NiO-CuO and $Ni_{1-x}Cr_xO_2$ thin films showed better electrocatalytic activity, lower charge transfer resistance, good stability, and resistant to poisoning effect as compare to pure NiO, CuO, and Cr_2O_3 thin films. These catalysts are less expensive and can be a good candidate for the direct methanol fuel cell.

Contents

Chapter,1 1

1 Introduction 1

1.1 Background and Motivation 1
1.2 Fuel cell 2
1.2.1 Types of Fuel cell 2
1.3 DMFC Current Challenges 12
1.4 Ceramic Material 13
1.4.1 Ceramic Oxide Thin Films 14
1.4.2 Thin Film Deposition Technique 15
1.5 Characterization Techniques 17
1.5.1 X-Ray Diffraction Spectroscopy (XRD) 17
1.5.2 Scanning Electron Microscopy (SEM) 19
1.5.3 Fourier Transform Infrared Spectroscopy (FT-IR) 20
1.6 Electrochemical Techniques 21
1.6.1 Cyclic Voltammetry (CV) 21
1.6.2 Chronoamperometry 23
1.6.3 Electrochemical Impedance Spectroscopy (EIS) 25
1.7 Research objectives 26

Chapter,2 27

2 Literature Review 27

Chapter,3 36

3 Experimental Work 36

3.1 Synthesis of ceramic oxide thin films 36
3.2 Characterization Instrumentations 40
3.3 Experimental Assembly 40

Chapter 4 42

4 Result and Discussion 42

4.1 Characterizations 42
4.1.1 X-ray Diffraction (XRD) 42
4.1.2 Scanning Electron Microscopy (SEM) 47
4.1.3 Fourier Transform Infrared Spectroscopy (FTIR) 45
4.1.4 Energy Dispersive X-Ray Spectroscopy (EDS) 48
4.1.5 Raman Spectroscopy 51
4.2 Electrochemical Studies 52
4.2.1 Linear Sweep Voltammetry (LSV) 52
4.2.2 Electrochemical Impedance Spectroscopy (EIS) 55
4.2.3 Chronoamperometry (CA) 57
Chapter 5 59
5 Conclusion 59
5.1 Summary 59
5.2 Future Recommendations 60
References 61

List of Figures

Figure 1.1. Illustrative Diagram of Alkaline Fuel Cell 3
Figure 1.2 Illustrative Diagram of Proton Exchange Membrane Fuel Cell 5
Figure 1.3 Illustrative Diagram of Phosphoric Acid Fuel Cell 6
Figure 1.4 Illustrative Diagram of Solid Oxide Fuel Cell.....8
Figure 1.5 Illustrative Diagram of Molten Carbonated Fuel Cell 9
Figure 1.6 Illustrative Diagram of Direct Methanol Fuel Cell.....11
Figure 1.7 Comparison of Different Types of Fuel Cells 12
Figure 1.8 Thin Film and Thick Film Rules 15
Figure 1.9 Sequential Steps in Dip Coating Method 17
Figure 1.10 Illustrative Diagram of X-Ray Diffractometer 18
Figure 1.11 Illustrative Diagram of Scanning Electron Microscope 20
Figure 1.12 Illustrative Diagram of FTIR 21
Figure 1.13 Potentiostatic Instrument Assembly 22
Figure 1.14 Conventional Cyclic Voltammogram 23
Figure 1.15 Schematic Diagram of Chronoamperometry Instrument.....24
Figure 1.16 Electrochemical Impedance Spectroscopy (Nyquist Plot) 25
Figure 3.1 Schematic diagram of Synthesis of Metal Oxide Thin Films.....37
Figure 3.2 Schematic diagram of Synthesis of Mixed Metal Oxide Thin Films 38
Figure 3.4 Three Electrode Electrochemical Cell 40
Figure 3.3 Potentiostate for Electrochemical Studies 41
Figure 4.1 XRD Pattern of FTO, NiO, CuO, NiO-CuO Thin Films.....43
Figure 4.2 XRD Pattern of NiO, Cr_2O_3, $Ni_{1-x}Cr_xO_2$ 44
Figure 4.3 SEM images of **a)** NiO **b)** CuO **c)** NiO-CuO thin films.....47
Figure 4.4 SEM images a) Cr_2O_3 b) $Ni_{1-x}Cr_xO_2$ thin films.....48
Figure 4.5 FTIR spectra of NiO, CuO, and NiO-CuO thin films.....46
Figure 4.6 FTIR spectra of Cr_2O_3 and $Ni_{1-x}Cr_xO_2$ thin films 46
Figure 4.7 EDS results of a) NiO, b) CuO, and c) NiO-CuO thin films 50
Figure 4.8 EDS results of a) Cr_2O_3 b) $Ni_{1-x}Cr_xO_2$.....50

Figure 4.9 Raman Spectra of NiO, CuO, and NiO-CuO thin films 51
Figure 4.10 Linear Sweep Voltammetry of a) NiO b) CuO c) NiO-CuO thin films at 0M, 0.1M, 0.2M, 0.3M methanol concentration d) Comparison of NiO, CuO, NiO-CuO thin films at 0.3M methanol concentration at $50mVs^{-1}$. 53
Figure 4.11 Linear Sweep Voltammetry of a) Cr_2O_3 b) $Ni_{1-x}Cr_xO_2$ thin films at 0M, 0.1M, 0.2M, 0.3M methanol concentration d) Comparison of Cr_2O_3 and $Ni_{1-x}Cr_xO_2$ at 0.3M methanol concentration.....54
Figure 4.12 EIS plot of $Ni_{1-x}Cr_xO_2$ thin film in 0.5 M NaOH before and after addition of 0.3 M methanol 56
Figure 4.13 EIS plot of NiO-CuO thin film in 0.5M NaOH before and after addition of 0.3M methanol 56
Figure 4.14 Chronoamperometric graph of NiO-CuO in 0.5M NaOH and 0.3M methanol 57
Figure 4.15 Chronoamperometric graph of $Ni_{1x}Cr_xO_2$ in 0.5 M NaOH and 0.3 M methanol.....58

List of Tables

Table 1 Ceramic Oxide Thin Films Synthesized 39
Table 2 Ceramic Oxide Thin Films Synthesized 39
Table 3 XRD Data of NiO, CuO and NiO-CuO Thin Films.....44
Table 4 XRD Data of Cr_2O_3 and $Ni_{1-x}Cr_xO_2$.....45

List of Abbreviations

AC	Alternating Current
CV	Cyclic Voltammetry
CA	Chronoamperometry
CE	Counter Electrode
CD	Current Density
DMFC	Direct Methanol Fuel Cell
EIS	Electrochemical Impedance Spectroscopy
FTIR	Fourier Transform Infrared Spectroscopy
GCE	Glassy Carbon Electrode
MOR	Methanol Oxidation Reaction
MFC	Microbial Fuel Cell
MCFC	Molten Carbonate Fuel Cell
OER	Oxygen Evolution Reaction
ORR	Oxygen Reduction Reaction
PAFC	Phosphoric Acid Fuel Cell
POFC	Phosphorus Oxide Fuel Cell
PEMFC	Polymer Electrolyte Membrane Fuel Cell
RE	Reference Electrode
SOFC	Solid Oxide Fuel Cell
SEM	Scanning Electron Microscopy
XRD	X-ray Diffraction

Chapter 1

1 Introduction

1.1 Background and Motivation

Due to the rapid increase in worldwide energy consumption and detrimental environmental emissions from conventional fossil fuel, alternative renewable and economical technologies for efficient energy conversions are demanded. Energy is a significant element for all human activities and advancements. One of the main future challenges of the earth will be energy, due to the growing global population and the advance lifestyles of individuals.[1]

Energy consumption is the measure of the country's economic growth and prosperity because it is a major factor for all developments. Our country Pakistan is facing serious energy shortage, it is because power supply and demand differences are big and are widening over time. In our country, energy crises have become critical as they rely solely on hydroelectricity and fossil fuel. The capacity of hydropower plants is extremely low to meet the increasing demands of electricity. Pakistan has limited resources of fossil fuel and needs to import to fill that void. Although the imported fossil fuels are providing enough amount of energy required, but at the same time life is endangered due to emission of toxic green-house gases (NO_X, SO_X) thus needs to be tackled by environment-friendly and renewable energy source. So, there is a need to put in place a resource for power generation that would not only satisfy the energy shortages but also offer a greener future with less toxic gases emission.[2]

Keeping all aspects under consideration, fuel cells are the best option for clean and safe power generation. Fuel cells with high efficiency, versatility in power supply, and low pollution emissions are attracting more attention to deal with this increasing energy

demand. Fuel cells undergo an electrochemical reaction to generate power with a smaller number of by-products as compared to the conventional energy conversion devices. They are expected to be suitable for use in transportation, stationary, and portable power generating devices.[1]

1.2 Fuel cell

A fuel cell is like a factory that continuously produces electricity as long as fuel and air are supplied as input. The fuel cell is similar to the battery as both undergo electrochemical reaction for direct electricity generation but unlike battery fuel cell is not consumed. Fuel cells can be preferred to batteries because they are more powerful and stable. The combustion process of the fuel cell is same as in the conventional heat engine but the fuel cell can carry out this process without heat production. Fuel cells supply power at low temperatures, more efficiently, and environment friendly. Fuel cells incorporate the benefits of both batteries and heat engines. Owing to these aspects it is predictable that fuel cells can significantly replace other devices. The general design of the fuel cell consists of three end-to-end sections: anode, electrolyte, and cathode. [3]

1.2.1 Types of Fuel cell

Depending on the form of electrolyte, there are several types of fuel cells; differing in their temperature range, power density, electrical performance, and common applications for which they are suitable. Types of fuel cells are as follows:[4, 5]

1.2.1.1 Alkaline Fuel Cell (AFC)

AFCs use alkaline electrolytes like KOH that have an advantage of faster oxygen reduction kinetics as compare to acidic media which makes them more efficient. Such fuel cells usually function at temperatures below 100 °C. In alkaline media OH ions are involved in oxygen reduction and hydrogen oxidation. The cathodic reduction of water produces OH ions which travel to the anode through the electrolyte, where they recombine with hydrogen by oxidation and produces water.[6]

At Anode:

$$H_2 + 2OH^- \longrightarrow 2H_2O + 2e^-$$

At Cathode:

$$1/2O_2 + H_2O + 2e^- \longrightarrow 2OH^-$$

Overall reaction:

$$H_2 + 1/2O_2 \longrightarrow H_2O$$

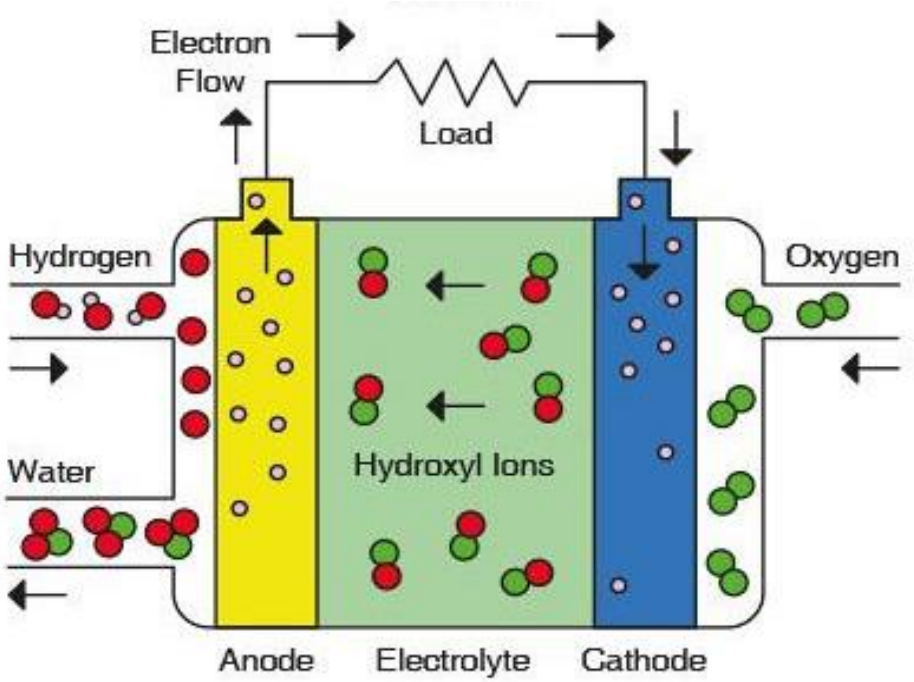

Figure 1.1. Illustrative Diagram of Alkaline Fuel Cell

This type of fuel cell was first used in space shuttles for energy production, producing drinkable water and cooling shuttle compartments. AFCs have multiple applications in space programs.[7]

1.2.1.2 Proton Exchange Membrane Fuel Cell (PEMFC)

Proton conducting polymer membrane is used as an electrolyte in PEM fuel cells. Usually operate at temperature range 80 °C – 105 °C. So, they are also low-temperature fuel cells because membranes are stable at a small temperature range. The major advancement in PEMFC is the use of the Nafion membrane which higher acidity, dual conductivity and is more stable than polystyrene sulfonate membranes. [8]The reaction of the PEM fuel cell takes place in acidic electrolytes. This type of cell converts hydrogen chemical energy into electrical energy by oxidation of hydrogen at anode producing photons that travel through membrane to the cathode. At cathode oxygen reduction occur which then recombine with protons and form water. [4]

At Anode:

$$H_2 \longrightarrow 2H^+ + 2e^-$$

At Cathode:

$$1/2O_2 + 2H^+ + 2e^- \longrightarrow H_2O$$

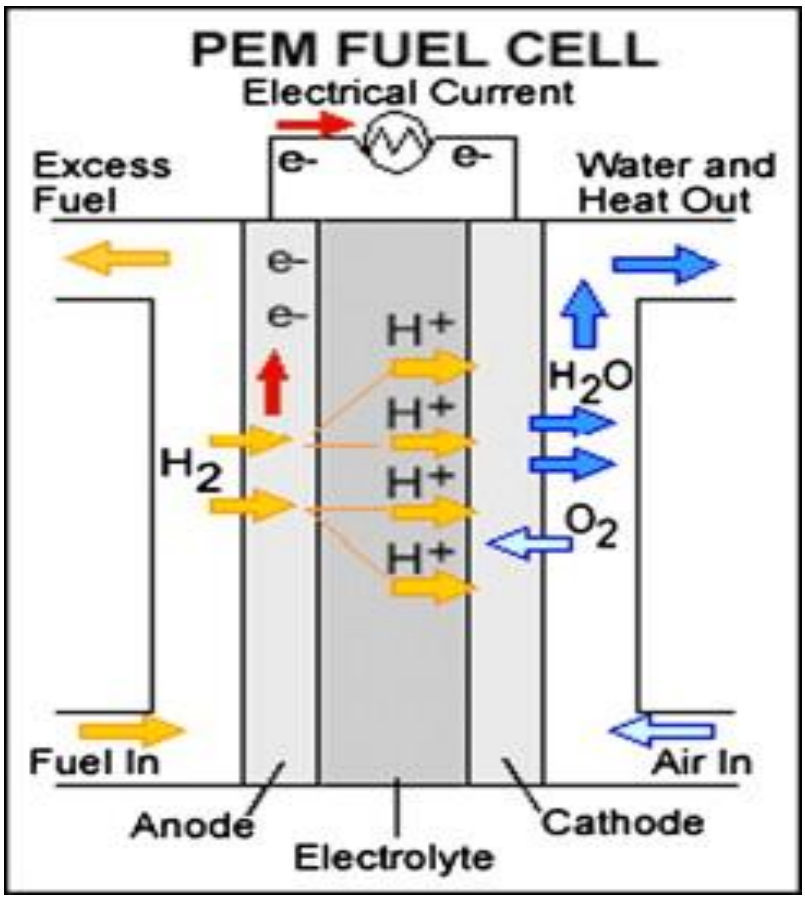

Figure 1.2 Illustrative Diagram of Proton Exchange Membrane Fuel Cell

The main application of PEMFCs is focused on transport vehicles as it has no harmful effect on the environment. Other applications are related to portable and stationary power generation.[9]

1.2.1.3 Phosphoric Acid Fuel Cell (PAFC)

Such cells employ phosphoric acid (85%) as an electrolyte which is stabilized in the SiC-based matrix. The reaction of these cells is the same as in proton exchange membrane fuel cells. The mostly used electrodes are platinum-based catalyst distributed on carbon-based support. Cathode reaction is comparatively faster than PEMFC because of its higher working temperature 150-200 °C. [10]

At Anode:

$$H_2 \longrightarrow 2H^+ + 2e^-$$

At Cathode:

$$1/2O_2 + 2H^+ + 2e^- \longrightarrow H_2O$$

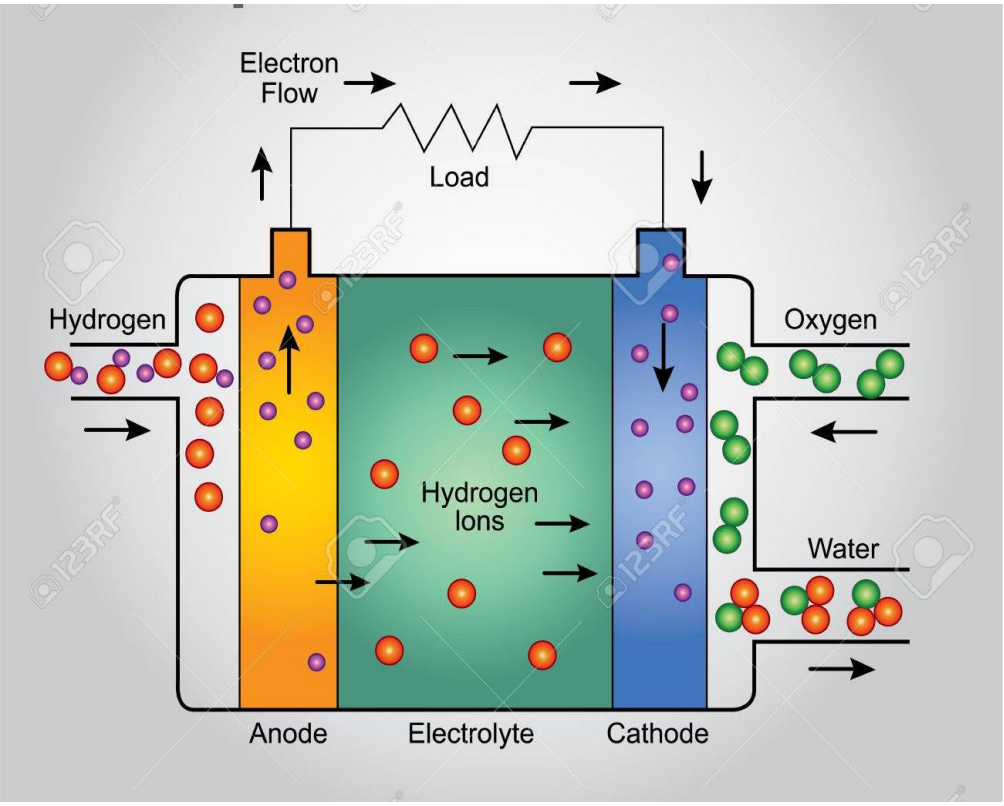

Figure 1.3 Illustrative Diagram of Phosphoric Acid Fuel Cell

As far as commercial development is concerned PAFC is most advanced. It is used worldwide for both stationary power plants: on-site power generation plants and distribution plants. These fuel cells are used for commercial systems due to its advantages like simple and easy construction, chemical and thermal stability, and high electrolyte stability at working temperatures 150-200 °C. [11]

1.2.1.4 Solid Oxide Fuel Cell (SOFC)

SOFCs are environment friendly and can attain an efficiency of 70%. Such cells have two phases of gas and solid as they use a solid oxide electrolyte which is more stable than MCFC because of no leakage. Oxygen ions formed at the cathode are transferred to the anode through the solid electrolyte. These oxygen ions migrate through solid by oxygen vacancies. Direct oxidation of fuel and partial oxidation of reforming reactions were observed at the anode.[12]

At Anode:

$$H_2 + O^{2-} \longrightarrow H_2O + 2e^-$$

At Cathode:

$$1/2O_2 + 2e^- \longrightarrow 2O^{2-}$$

Many issues with this device are due to high-temperature conditions which can cause mechanical and chemical stability problems. It is preferred to operate this cell at a low temperature for better conductivity or choose some suitable materials with high thermal and chemical stability.[13]

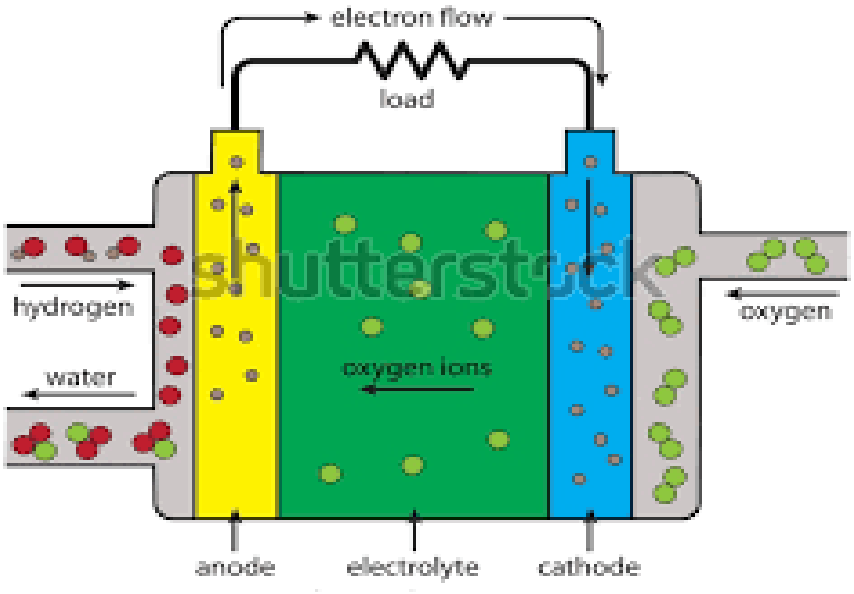

Figure 1.4 Illustrative Diagram of Solid Oxide Fuel Cell

1.2.1.5 Molten Carbonated Fuel Cell (MCFC)

Molten carbonated fuel cell is a very obvious choice for carbonaceous fuels that produce CO_2 on oxidation. Molten carbonates usually LiNa or LiK carbonates are used as electrolytes stabilized in the matrix and entrapped between electrodes. Carbonate ions produced at cathode travel to the anode through the electrolyte where they are used for hydrogen oxidation. Anode also takes part in other internal reforming reactions.

At Anode:

$$H_2 + CO_3^{2-} \longrightarrow H_2O + CO_2 + 2e^-$$

At Cathode:

$$1/2O_2 + CO_2 + 2e^- \longrightarrow CO_3^{2-}$$

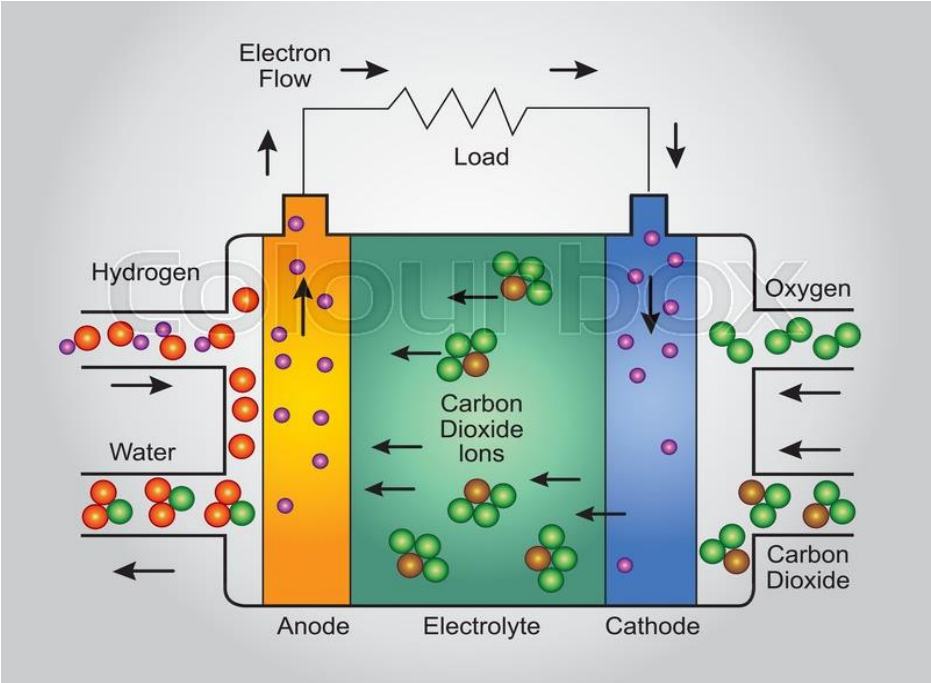

Figure 1.5 Illustrative Diagram of Molten Carbonated Fuel Cell

These cells can achieve 50-70% output efficiency when another power generator is attached. Advantages of these fuel cells are:

- It reforms methane internally due to high-temperature conditions (600-700 °C).
- The waste heat of the cell can be directly used by the combined cycle.
- Oxygen reduction kinetics increases due to high temperatures.

These cells are used in stationary power systems because of their high efficiency and high-grade heat production.[14]

1.2.1.6 Direct Methanol Fuel Cell (DMFC)

Direct methanol fuel cells (DMFCs) are thought to be the most promising green among other fuel cells because of their high energy density and pollution-free emissions.[15, 16] These cells are PEM technology-based low-temperature fuel cells using methanol as fuel. They operate at the same temperature (80-105 °C) as PEMFCs, while DMFCs can also operate at higher temperatures depending on electrolyte material.

DMFCs are mainly classified into two types based on the style of fuel supply:

- Active DMFCs: These cells include additional components like pumps, blowers, and fans for supplying and removing reactants and products.
- Passive DMFCs: These cells have simple structures; don't need any extra component. They rely on passive processes like gravitation, natural convection, diffusion, and capillary action to carry methanol and oxygen.

In DMFC methanol is directly subjected into the cell eliminating the intermediate step of steam reforming of methanol. In DMFC the energy is produced by electrooxidation of methanol at the anode. Methanol is relatively preferred because it is readily derived from biomass supplies or natural gas and have high theoretical energy density. [4] Additionally, methanol is easy to handle, cost-effective, less toxic, and has high energy storage capacity.[17]

It mainly consists of cathode plate, anode plate, and membrane electrode assembly separating both electrodes. Methanol and water are subjected directly to the anode where methanol oxidation reaction (MOR) takes place in several steps generating protons, electrons, carbon dioxide, and heat. Protons and electrons migrate to the cathode through electrolyte and external circuits respectively. At cathode atmospheric oxygen, protons and electrons combine to produce water and heat which is called oxygen reduction reaction (ORR). The reactions are: [18]

At Anode:

$$CH_3OH + H_2O \longrightarrow CO_2 + 6H^+ + 6e^- + \text{Heat}$$

At Cathode:

$$3/2O_2 + 6H^+ + 6e^- \longrightarrow 3H_2O + \text{Heat}$$

Overall reaction:

$$CH_3OH + 3/2O_2 \longrightarrow CO_2 + 2\,H_2O + \text{Heat}$$

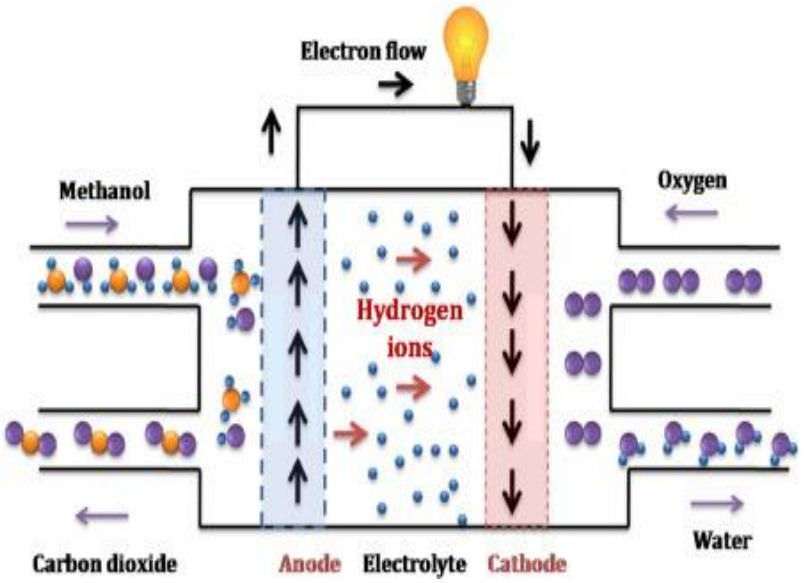

Figure 1.6 Illustrative Diagram of Direct Methanol Fuel Cell

DMFC is appropriate for modern life as it has suitable characteristics for portable devices and helpful in terms of liquid fuel storage, transport, and usage.[15] [19]

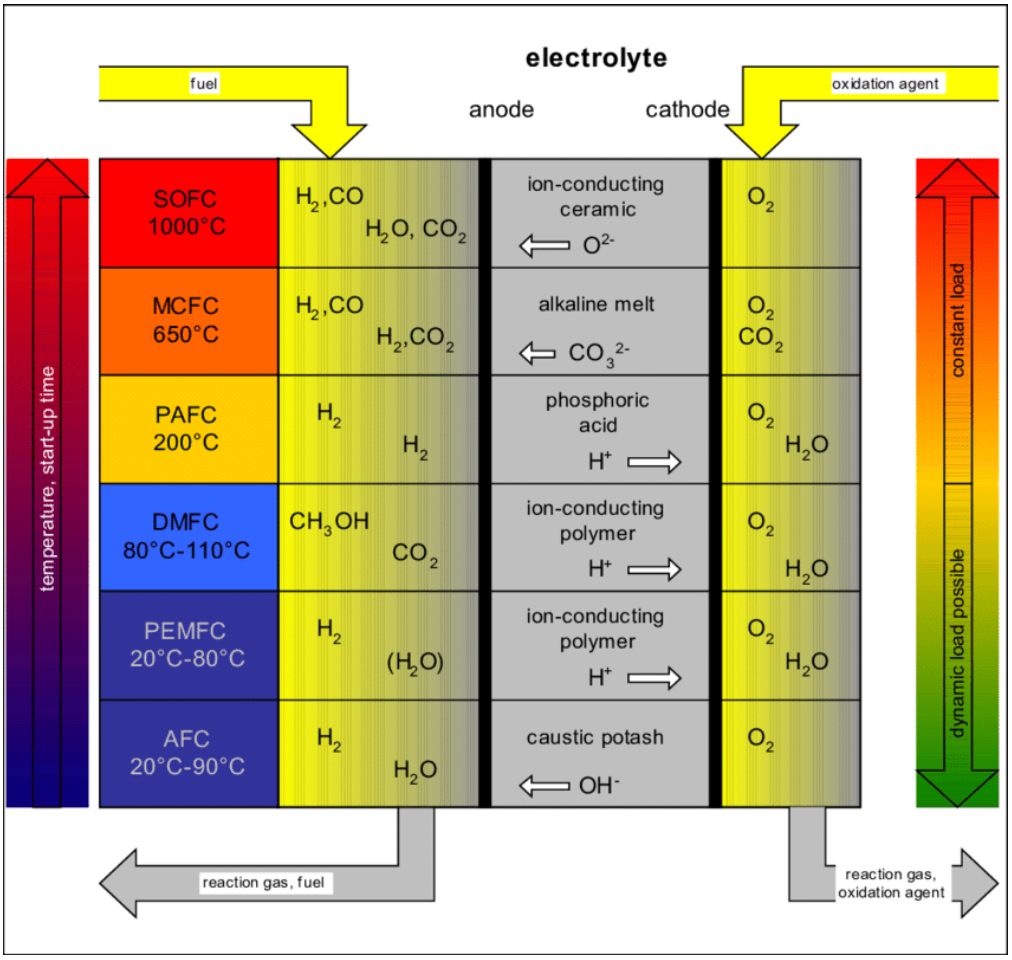

Figure 1.7 Comparison of Different Types of Fuel Cells

1.3 DMFC Current Challenges

Despite these advantages, the major constraints for the commercialization of DMFC are:[16]

- methanol cross-over from anode to cathode
- slow anodic kinetics
- high cost

Nowadays in most of DMFCs electrolyte membrane is used in conjunction with PEM to boost their efficiency. This combination blends the benefits of both PEMFC and DMFC. Such membranes can enhance protons conductivity but are not suitable for methanol

blocking. Methanol crossover from anode to cathode is a serious issue as it significantly reduces current density, cell voltage, and fuel consumption and therefore cell efficiency. Nafion based membranes are being used that reduces methanol crossover but cannot cut cost. Commonly dilute methanol solutions are used to reduce methanol crossover. A specific approach to deal with this problem is the development of methanol tolerant cathode.[4]

Heat control is another problem that needs to be tackled in this system, as the temperature of the system increases with increasing methanol crossovers. This ultimately reduces the overall response rate due to an increase in activation over-potential. This limits the electrode response rate that affects the system's voltage output. Less than 30% of methanol's total chemical energy can be used as electricity, while the rest is converted into heat. [20]

Cost of DMFCs production, energy consumption, and profitability in the market are major targets for every manufacturer. One of the key barriers to DMFC's entering commercialization is the need for platinum catalysts to achieve enough power density. Two approaches were implemented to lessen the expense of catalysts for the fuel cell are investigating non-noble catalysts or reduce the platinum loading. [19, 21]

1.4 Ceramic Material

Ceramic materials are based on inorganic non-metallic compounds often oxides, nitrides, and carbides. Essentially ionic and covalent compounds that makeup ceramics are compounds formed between metals and non-metals. The crystallinity of ceramics varies from a highly ordered structure to amorphous. The useful properties of ceramics are toughness, hardness, chemical inertness, and low thermal and electrical conductivity. Ceramics and its composites in the form of powder, thin-film, and single-crystal play an important role in electrical, chemical, pharmaceutical, and industrial sectors.[22, 23]

Ceramics can be divided into two major groups:

- structural ceramics
- functional ceramics.

Structural ceramics can withstand mechanical loads and severe chemical and thermal conditions. These ceramics are used for high-performance applications like metal cutting and tools shaping.

Functional ceramics have good optical, electrical, and magnetic properties that are commonly used in sensors, optics, catalysis, photovoltaics, and environmental applications, etc. Functional ceramics also attract the interest of researchers as they can interact with the environment to respond or generate power. Functional metal oxides and halides play an important role in the field of electrochemistry and catalysis due to their bonding and structure. [24]

Since much of the metallic element is reactive to oxygen and oxides are found in stable single or mixed phases. Oxides are the main group of ceramics with chemical inertness, thermal stability, and oxidation-resistant properties. [25]Metal oxide nanoparticles have attracted growing technological and industrial interest due to their optical, catalytic, electrical, and magnetic properties.[26]

1.4.1 Ceramic Oxide Thin Films

Thin film technology is the basis of the surprising advances in solid-state electronics. The importance of the optical properties of ceramic or semiconductor and their activity in two-dimensional structures are responsible for the great interest in the science of thin films. The study of thin films depends on the geometry and the thickness of films. Amorphous or crystalline thin films are formed by using different deposition techniques either by physical or chemical methods.[27]

The thin films are defined as thin layers of the material that varies from 5 nanometers to 2 micrometer and thick films vary from tens to hundreds of micrometers. The key difference between the thin film and thick film is the thickness of the layers deposited.[28]

Thin-film deposition requires the deposition of individual atoms or molecules on the surface while the thick film deals with particle deposition. Thin-film formation alters the chemical, physical properties, and surface morphology of the materials without altering the properties of the bulk material. So, thin films exhibit specific material properties that are substantially different from the corresponding mass. This is due to their dimensional restriction, microstructure, geometry, and associated metallurgy. This is due to the immense rise in the surface to volume ratio induced by the dimensional constraints.[29] [30]

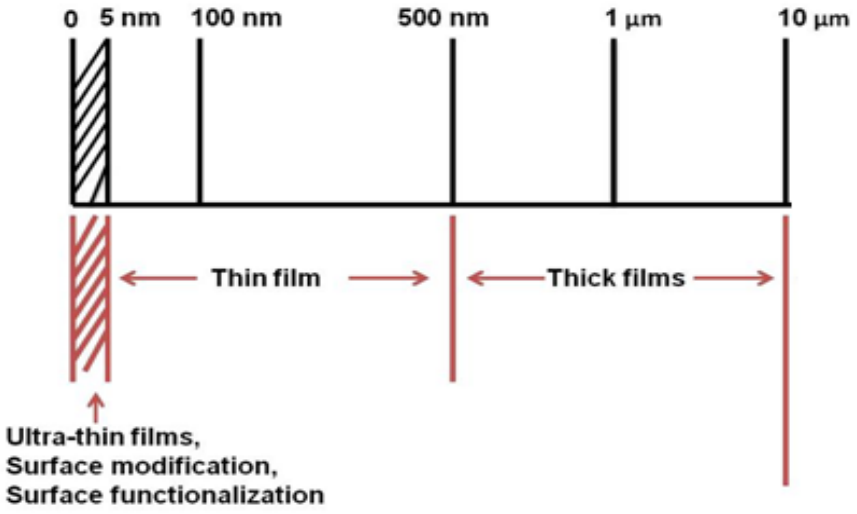

Figure 1.8 Thin Film and Thick Film Rules

1.4.2 Thin Film Deposition Technique

All deposition techniques essentially require three separate steps which are:

1. Production of necessary constituents like atoms, ions, or molecules.
2. Transport of these species to the substrate through a suitable medium.
3. Deposition of those species on the substrate.

The technique used in this research for metal oxide thin film deposition on a glass substrate is dip coating.[31]

1.4.2.1 Dip Coating

It is a simple, versatile, and cost-effective method of solution deposition that enables coating of wide areas and complex shape substrates. Dipping can be either automatic or manual. [32]The dip-coating process for thick and thin film preparation consists of several successive steps. At first, the substrate must be immersed in the precursor solution to be coated with same speed. The substrate is lifted from the prepared solution with the same speed after staying inside the solution for some time, so a thin layer can form on the substrate. After the excess liquid is drained off the substrate the solvent evaporates from the surface creating a thin layer. The film formed is then stabilized by associated chemical reactions and drying. [33]

The film-forming process follows the fluid mechanical equilibrium between receding liquid and the suspended film. That mechanical equilibrium is regulated by many forces. The most important role is played by viscous drag, surface tension, and gravitational force.[34]

The thickness of the film is also controlled by competition between these forces in the film deposition area. The properties and thickness of the film depend on some parameters like withdrawal speed, number of cycles, immersion time, solution composition, temperature, and humidity, etc. [35]

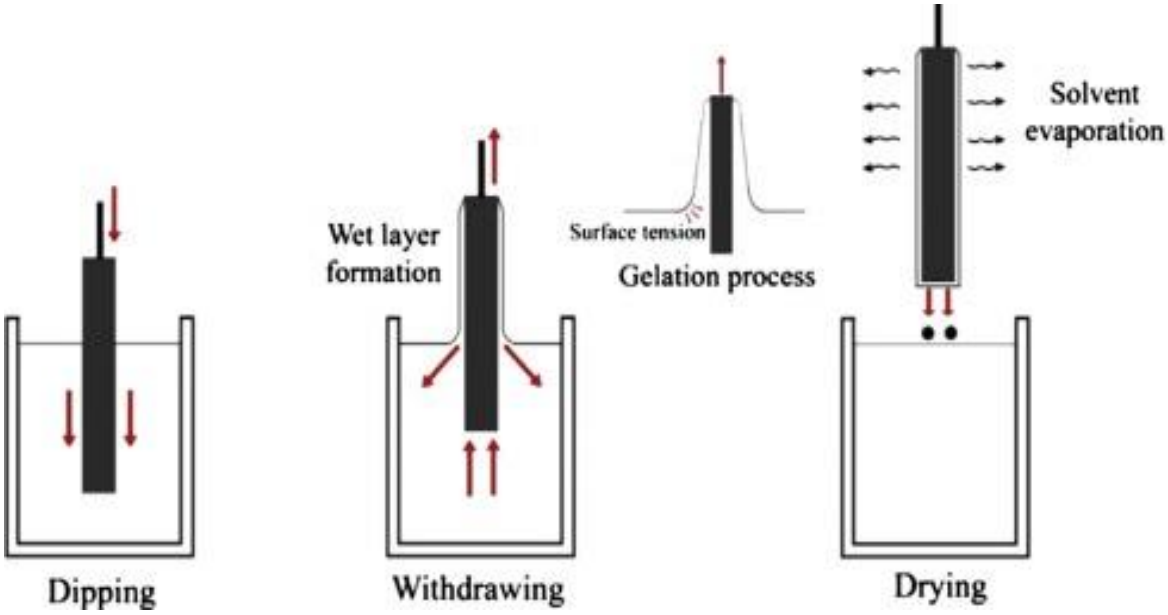

Figure 1.9 Sequential Steps in Dip Coating Method

1.5 Characterization Techniques

1.5.1 X-Ray Diffraction Spectroscopy (XRD)

X-ray diffraction (XRD) is an effective and non-destructive analysis technique for the characterization of crystalline material. This method is used to identify the sample purity, structure, phase, desired crystal orientation, and other lattice parameters like average grain size, strain, crystallinity, and crystal defects. [36]The sample to be studied should be finely grounded, homogenized, and average bulk composition. XRD's basic principle is based upon the constructive interference of the sample being investigated with monochromatic X-rays. X-rays are produced in cathode ray tube and then screened through a monochromator to produce monochromatic rays and are incident on the sample. Crystalline material serves as 3D grating for X-rays wavelength equivalent to the lattice

spacing of crystal planes. XRD peaks are formed from monochromatic ray's constructive interference after being scattered at different angles from lattice planes of crystals. The peak intensities are determined by the position of atoms in lattice planes. Thus, the characteristic XRD pattern reflects the fingerprint of the atomic arrangement in the sample.[37]

Constructive interference takes place when rays diffracted from the sample satisfy Bragg's law:

$$2d\sin\theta = n\lambda$$

λ= wavelength

d= interlayer distance

n= no. of layers under consideration

XRD is designed to ensure the best possible quality of diffraction data can be obtained. It comprises of three main components a sample holder, cathode ray tube, and X-ray detector. The X-ray diffractometer has simple geometry in which sample material rotates at the position where incident rays are focused.

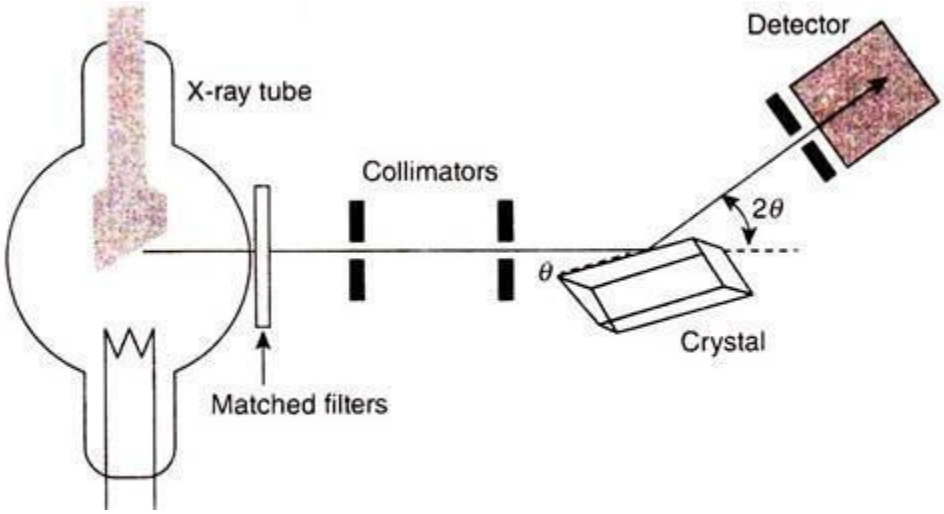

Figure 1.10 Illustrative Diagram of X-Ray Diffractometer

1.5.2 Scanning Electron Microscopy (SEM)

SEM is a microscope that uses a beam of electrons to produce an image instead of light. This technique is used to scan the focused beam of electrons over the sample surface for interaction to create a higher resolution image of surface morphology and shape of the crystals used effectively in the microanalysis of microstructures. It works on the fundamental principle that electrons carry a definite amount of kinetic energy that is used to generate different types of signals by an interaction between sample and electrons at the time of deceleration of incident electrons at the solid-state sample. These signals often carry secondary electrons forming an image, as well as providing the structure of crystalline material and orientation of material by backscattered electrons (BSE).[38]

The energy-dispersive X-ray spectroscopy (EDS) analytical technique is widely used in combination with SEM that offers information about elemental surface composition based on X-rays emitted from various points of the sample surface under analysis. Thus, the SEM's imaging capabilities coupled with EDS elemental analysis can, therefore, be used to obtain both physical and chemical information of the sample.

Its key components are the vacuum system, scanning system, electron column, monitor, and detectors.

SEM analysis is a non-destructive technique because electrons do not penetrate the sample while interacting with the sample surface allowing repeated analysis of the material. It works quickly as it takes less than five minutes to complete BSE, EDS, and SEI. It can detect fractures and gives information about topography, composition, morphology.[39]

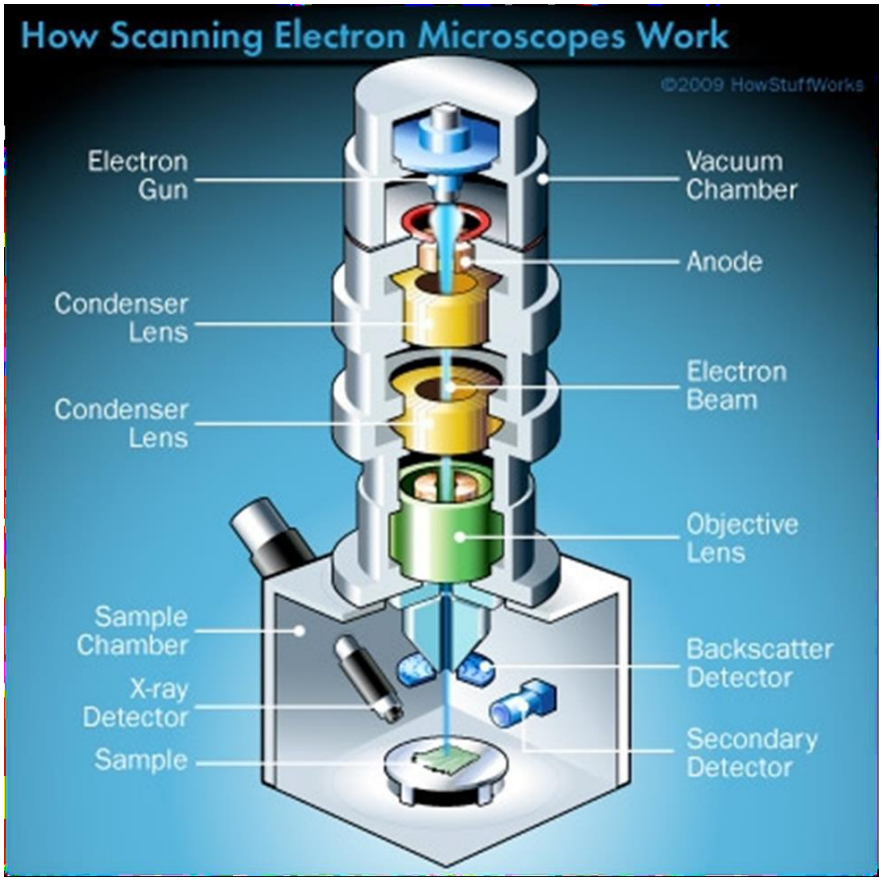

Figure 1.11 Illustrative Diagram of Scanning Electron Microscope

1.5.3 Fourier Transform Infrared Spectroscopy (FTIR)

This technique is named Fourier Transform Infrared Spectroscopy (FTIR) as it is useful in combination with Fourier Transformer, which converts the raw data into a spectrum. This technique can be used to obtain the absorption or emission IR spectrum of a substance under analysis in any physical state i.e., solid, liquid, or gas. FTIR is aa analytical technique constructed for the measurement of the absorption of electromagnetic radiation wavelengths within the range of infrared radiations (4000-400 cm−1). The radiations absorbed by the sample are converted into vibrational and rotational energy. The signal generated at the detector presents as a spectrum. The resulting spectrum gives information

about chemical structure and interactions by bands position relative to the strengths and presence of bonds for different functional groups or class of compounds. Every molecule and chemical structure produce a specific spectral fingerprint so FTIR analysis can identify them. [40]

The basic setup and working of FTIR are shown below:

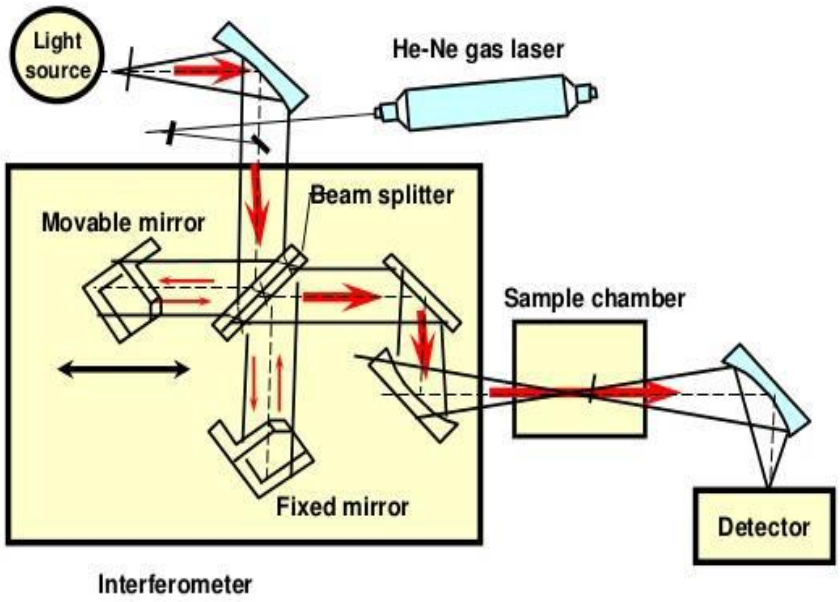

Figure 1.12 Illustrative Diagram of FTIR

1.6 Electrochemical Techniques

1.6.1 Cyclic Voltammetry (CV)

Cyclic voltammetry (CV) is commonly used most effective electrochemical technique to study the reduction and oxidation reactions of molecular species. It is also helpful for the investigation of electron transfer chemical reactions like catalysis. This may be the most

adaptable electrochemical method to test the activity of electroactive species. Its adaptability and simplicity of measuring results in its widespread use in the field of electrochemistry, organic, inorganic and biochemistry, etc.[41]

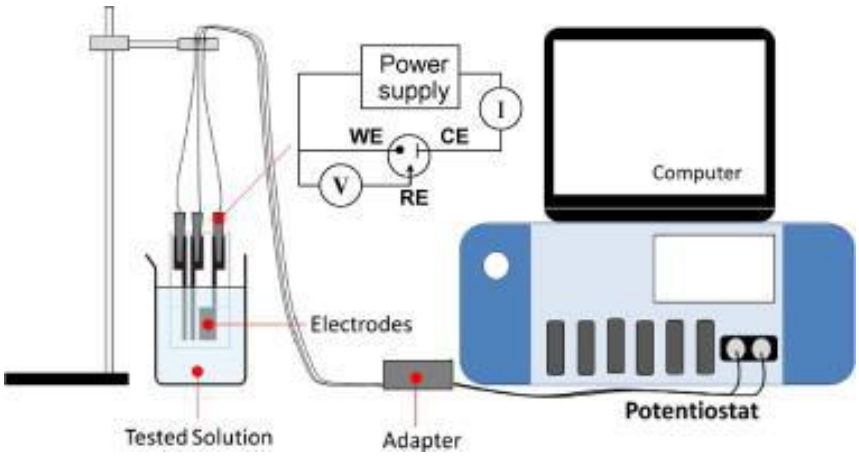

Figure 1.13 Potentiostatic Instrument Assembly

Mainly CV is used to analyze the electrochemical properties of the solution analyte. For the CV experiment, there is an electrochemical cell comprising three electrodes, namely the working electrode, the counter electrode, and the reference electrode.

The working electrode performs electrochemical reactions of our interest. The potential applied across working electrode as a function of reference electrode is monitored by potentiostat. From experiment-to-experiment different types of the working electrode can be used to promote surface adsorption of the specie and provide a specific potential window. A reference electrode in an electrochemical cell is used as a reference to measure the potential of another electrode because it has a potentially definite and stable equilibrium. Commonly used reference electrodes are Ag/AgCl electrode, Saturated Calomel Electrode (SCE), and Standard Hydrogen Electrode (SHE). The counter electrode has task of completing the electrical circuit. Usually, the platinum disk or wire is used as a counter electrode. To increase the conductivity of a solution a large

concentration of the electrolyte is required. As electrons transfer occurs at electrodes the supporting electrolyte will migrate to complete the circuit and balance the charge.[42]

The cyclic voltammogram is a representation of current versus potential. In cyclic voltammograms, working electrode potential is encouraged to ramp in a backward direction to reach the initial point after achieving the defined potential during the experiment. Cyclic voltammogram is obtained during the potential scan, by measurement of current at the working electrode.[43]

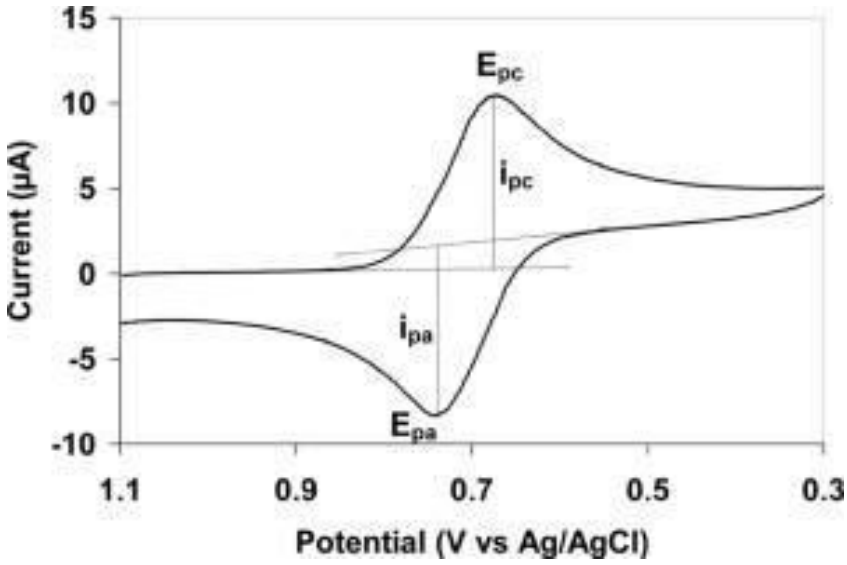

Figure 1.14 Conventional Cyclic Voltammogram

1.6.2 Chronoamperometry

Chronoamperometry is a time-dependent electrochemical technique in which working electrode potential is increased and the resultant current passing through the cell is monitored carefully with time. This technique is performed to study the electrochemical activity and stability of electrocatalyst. [44]

The three-electrode system used for this technique is similar to those used for CV and EIS. For chronoamperometry, an extended time is needed to evaluate material sustainability. Mostly a fixed region of the electrode is used which is appropriate for electrode processes of coupled chemical reactions. A fixed potential is applied for a particular period in a given time to carry out the analysis. This technique gives a better signal to noise ratio as the current is integrated for longer time intervals compared to other amperometry techniques used for this purpose.[45]

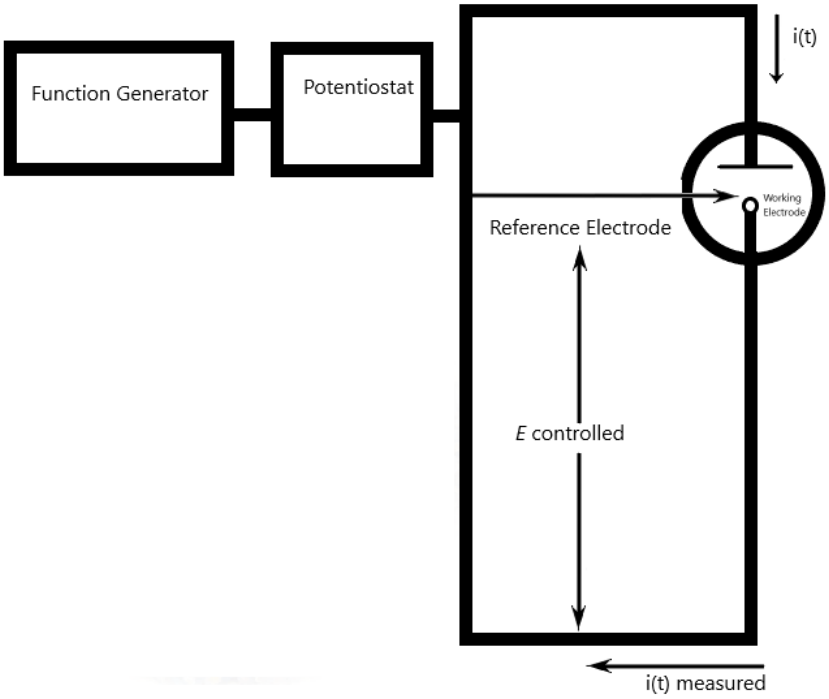

Figure 1.15 Schematic Diagram of Chronoamperometry Instrument

1.6.3 Electrochemical Impedance Spectroscopy (EIS)

The measure of capability of the circuit to resist the flow is called impedance. This refers to the frequency-dependent resistance. It is given by AC of a specific frequency in hertz.

$$Z\omega=E\omega/\omega$$

EIS measurements are done by applying sinusoidal voltage or current at a fixed frequency range and then the response is observed at each frequency. EIS data are either presented as a Nyquist plot or Bode plot. Mostly impedance studies consider Nyquist plot.

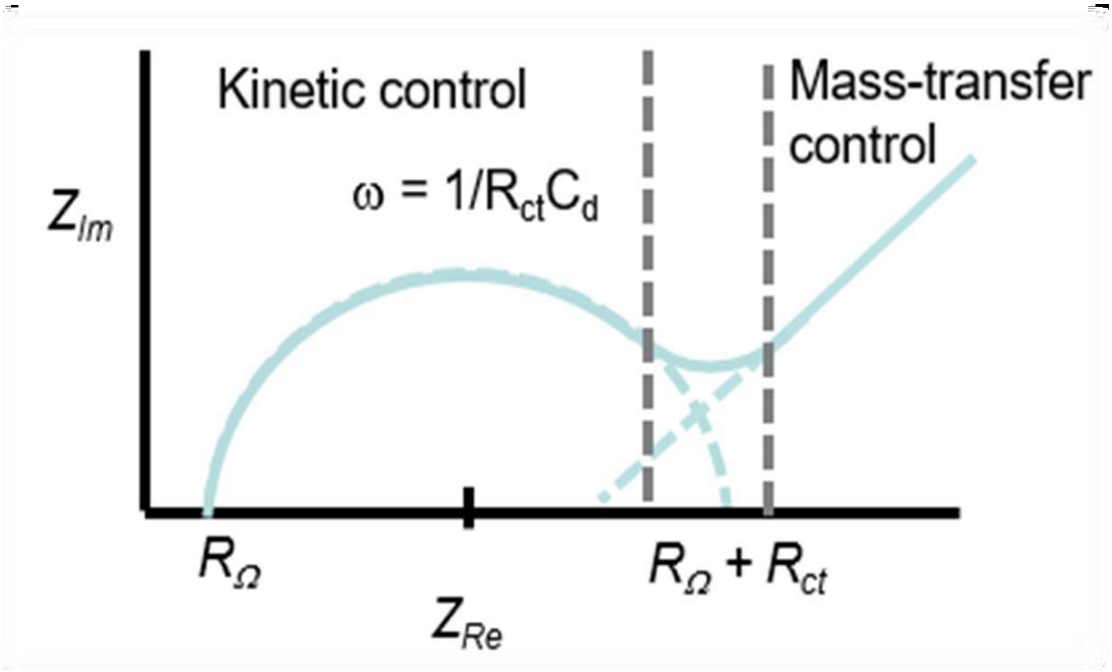

Figure 1.16 Electrochemical Impedance Spectroscopy (Nyquist Plot)

The setup used to run EIS is the same as that for CV. Only we need to decide, whether we want to run it on potentiostatic mode or galvanostatic mode.

EIS information helps to differentiate between electrochemical processes. It can help identify diffusion-limited processes. It provides information about the capacitive behavior of the electrode. Thus, giving off information about the overall reaction rate of the electrochemical process occurring on that electrode. It is also useful in corrosion studies of the metallic electrodes. [46]

1.7 Research objectives

The research is based on following objectives:

- Synthesis of ceramic films by dip coating method.
- Characterization of synthesized catalyst via XRD, SEM and FTIR.
- Optimization of different parameters such as concentration and solvent
- Study of electrochemical activity of synthesized catalyst through linear sweep voltammetry for methanol oxidation.
- Measurement of charge transfer parameter

Chapter 2

2 Literature Review

I. Danaee et al. [2009] reported a nickel and nickel-manganese alloy film synthesized on the graphite surface by using galvanostatic deposition technique and tested for methanol electro-oxidation in alkaline media. The catalytic activities and redox process was analyzed by methods of CV, CA, and EIS that were used for analysis. The CV data presented that the graphite modified electrodes show electrocatalytic activity at approximately 650mV versus Ag/AgCl, while the bare graphite electrode didn't show any activity. The response to methanol oxidation by G/NiMn alloy electrode significantly higher as compares to G/Ni electrode**.** It was proposed that the reason of higher activity of G/NiMn was methanol pre-absorption on Mn-sites due to their interaction between lone pair of oxygen atom in methanol molecule and partially filled d-orbital of manganese species. Double step CA of G/NiMn electrode indicated irreversible process and diffusion-controlled process was dominant. The coefficient of diffusion of methanol was 4×10^{-6} cm^2s^{-1}.[47]

Yaojuan Hu et al. [2014] reported Pt-Ni catalysts synthesis supported on graphene by using a controlled galvanostatic replacement method at room temperature using different molar ratios of precursors $PtCl_6^{2-}/Ni^{2+}$.The hollow nanostructure Pt-Ni/graphene nano-catalyst was fabricated by a molar ratio of 3:1. The catalysts synthesized were characterized by X-ray diffraction spectroscopy (XRD), transmission electron microscope (TEM), and energy-dispersive X-ray spectroscopy (EDS). The stability and electro-catalytic performance of hollow Pt-Ni/graphene nano-catalyst for methanol electro-oxidation reaction were higher than the dense Pt-Ni/graphene catalyst. The improved electrocatalytic performance of hollow nanostructured Pt-Ni/graphene is due to its greater

electrochemically active surface area and the synergistic effect of metals Pt and Ni in the catalyst.[48]

Shengnan Sun et al. [2015] reported Ni-Co oxides and hydroxide catalysts synthesis with different compositions on stainless steel mesh by using the co-electrodeposition technique. Ni-Co hydroxide catalyst with different atomic ratios of Ni and Co hydroxides were prepared by using different concentrations of precursors $Ni(NO_3)_2$ and $Co(NO_3)_2$. Ni-Co oxide catalysts were prepared by annealing of hydroxide catalysts. The electrocatalytic activity for methanol oxidation was analyzed by using CV at voltages from -0.1 V to 0.6 V vs. Hg/HgCl in 1.0 Molar KOH solution. The methanol oxidation reaction performance of Ni-Co oxides was observed to be higher than Ni-Co hydroxides. The MOR performance increases by increasing the content of Ni metal, but the highest activity and lower charge transfer resistance (Rct) was found at Ni 46% composition. Higher MOR activity of Ni-Co oxides was due to synergistic role of both metals in spinal structure. [49]

H.B. Hassan et al. [2018] reported synthesis of nanocomposites of Ni-metal oxides (Fe2O3, Co3O4, ZnO, and MnO2) by electrodeposition method on the carbon substrate. The elemental composition and surface morphology of the nano-catalysts was analyzed by using EDS, SEM, and XRD techniques. The study of electrochemical catalytic activity by nanocomposite was carried out by cyclic voltammetry (CV), impedance spectroscopy (EIS) and chronoamperometry (CA). All of the prepared nanocomposites showed better catalytic activity, higher stability, and lower charge transfer resistance as compare to Ni on the carbon substrate. The order of catalysts toward electrooxidation performance is Ni-Fe2O3/C > Ni-ZnO/C > Ni-Co3O4/C > Ni-MnO2/C > Ni/C. This improved catalytic activity of nanocomposites can be due to the synergistic effect of mixed oxides. The maximum current density of 339 and 302mAcm^{-2} was observed by Ni- Fe_2O_3/C catalyst at 1.0M methanol and 1.0M ethanol respectively. Moreover, it showed lower R_{ct} values of 6.2 and 10.7 Ωcm^2 for methanol and ethanol electro-oxidation.[50]

Pengcheng Wang et al. [2016] reported homogeneously dispersed NiO nanoparticles deposited on nitrogen-doped carbon nanotubes synthesized through the process of chemical precipitation followed by calcination. Samples were prepared with different calcination temperatures (200, 300, 400, 500°C) and different NiO contents (3X, 5X). The morphology of synthesized composites was characterized by XRD, TEM, and XPS. The techniques of cyclic voltammetry and chronoamperometry were used to examine the electrochemical efficiency of catalysts. The results showed the effect of calcination temperature, doped nitrogen, and NiO content on electrocatalytic activity for MOR. The best electrocatalytic performance was presented by an optimized NiO-NCNT-3X-400 catalyst with improved stability, rapid charge transfer, and excellent availability for the methanol electro-oxidation reaction. [1]

I. Danaee et al. [2008] reported the synthesis of Ni and NiCu alloy electrodes on glassy carbon surface by an electrochemical deposition method. Methods of CV and CA were used for investigation of the oxidation-reduction process and electrocatalytic activities toward methanol oxidation reaction in alkaline solution. The CV results of NiCu alloy shows the formation of Ni oxyhydroxide ß/ß crystallographic form under repeated potential cycling. NiCu/GC catalyst in the presence of 0.3M methanol shows significantly higher current density at 650mV vs Ag/AgCl as compare to Ni/GC, because of the higher surface area of Ni oxyhydroxide. The rise in anodic peak current is associated with a drop in cathodic peak current. The anodic peak currents of NiCu/GC were directly proportional to the square root of the scan rate. In CA studies the diffusion coefficient was observed to be $2\times10^{-6}cm^2s^{-1}$ in agreement with CV measurements.[51]

R.H. Tammam et al. [2013] studied methanol electrooxidation performance of catalysts consisting of MnO_x and NiO_x nanoparticles on a glassy carbon electrode with different arrangements. Electrochemical and surface analysis was made by techniques CV, EIS, and SEM. The improvement in catalytic activity was dependent on the structure and content of NiO_x nanoparticles. The catalyst $GC/MnO_x/NiO_x$ in which NiO_x is deposited after MnO_x deposition on the GC electrode displayed the best performance for methanol electro-oxidation in an alkaline medium. The order electrochemical activity of the

catalysts prepared was observed as $GC/MnO_x/NiO_x$ > GC/NiO_x > $GC/NiO_x/MnO_x$. Synergism between NiO_x and MnO_x was proposed and this synergistic role of both metal oxides was primarily due to the higher absorbability of methanol on MnOx. An optimum minimum amount of loading of NiO_x was observed in $GC/MnO_x/NiO_x$ to achieve a higher rate of methanol electrooxidation. The EIS measurements were as per CV results and supported the observations.[52]

Guang-Ya Hou et al. [2015] reported a study in which they have fabricated Ni-Ti-O nanotubes array by anodizing NiTi alloy using the solution with glycerol and ethylene glycol as anodization media. Subsequently, Ni-Ti-O nanotubes were annealed under the hydrogen atmosphere leading to substantial improvement in electrocatalytic activity. The characterization of Ni-Ti-O NTs before and after annealing treatment was made by SEM, XPS, and XRD techniques. Electrocatalytic results obtained from CV and EIS showed that Ni-Ti-O NTs annealed at 500°C for 2 hours under hydrogen have excellent activity and stability for methanol oxidation reaction in KOH solution. This improvement in electrocatalytic performance was due to increase in active sites and conductivity of electrode provided by the reduction reaction of Ni^{+3}. The current density of the electrode increases after 1000 consecutive cycles and shows small variation after placing the electrode in the air for 30 days. Consequently, the Ni-Ti-O NT/Ni-Ti electrode had long term stability for methanol oxidation and be used practically in direct methanol fuel cells. [16]

M.A. Abdel Rahim et al. [2005] stated the study of Ni and Ru catalytic performance toward methanol electrooxidation. Various catalysts were synthesized by using a potentiostatic deposition method with different ratios of Ni and Ru deposited on the graphite electrode by relatively changing the concentrations of metal salts in a deposition bath. The deposition method and different compositions both influenced the catalytic activity as the relative dispersal of Ni and Ru depends on electro-deposition. Electrochemical results displayed that the catalysts prepared with extra Ni deposition time and with simultaneous deposition of Ni, Ru showed higher current density. Based on

results, it was concluded that methanol oxidation takes place at Ni and intermediate oxidation at Ru. [17]

H. B. Hassan et al. [2015] reported the preparation of pure Ni and Ni-MgO composite catalysts on carbon substrate by the galvanostatic deposition technique. Ni-MgO composite was deposited on a carbon substrate by electrodeposition in the presence of MgO reinforcement particles in the Nickel Watt bath. The efficiency of Ni/C and Ni-MgO/C electrocatalysts for methanol and ethanol oxidation was studied and compared. These electrocatalyst's composition, surface morphology, and structure were analyzed by EDS, SEM, and XRD. The electrochemical techniques used for the measurement of electrocatalytic performance of prepared electrodes were CV, CA, and EIS. The electrocatalytic efficiency of the Ni-MgO /C anodes prepared by deposition at various current densities (10, 20, 40, 80 $mAcm^{-2}$) was compared with the catalytic activity of pure Ni/C anodes prepared under the similar conditions. Ni-MgO /C electrode fabricated at 40 $mAcm^{-2}$ showed anodic peak current 176 $mAcm^{-2}$ for ethanol and 196 $mAcm^{-2}$ for methanol. While pure Ni /C electrode fabricated at 40 $mAcm^{-2}$ showed a peak current density of 65 $mAcm^{-2}$ for methanol and 60 $mAcm^{-2}$ for ethanol. The addition of MgO greatly enhanced the methanol oxidation catalytic activity of Ni and improved its susceptibility to poisoning. The findings of EIS supported the CV measurements and showed lower R_{ct} and improved the roughness of Ni-MgO /C electrodes. [53]

M.U. Anu Prathap et al. [2013] synthesized $NiCo_2O_4$ electrocatalyst through a hydrothermal method in presence of urea. The characterizations were carried out by XRD, nitrogen adsorption, SEM, and BET method. Electrocatalytic activity of $NiCo_2O_4$ for methanol oxidation in alkaline solution was measured by using CV and CA and compared with NiO and Co_3O4 electrodes. For methanol electrooxidation, a thorough analysis was carried out by changing parameters like methanol concentration and potential scan rate. Electrocatalytic activity for methanol oxidation by the modified electrode of $NiCo_2O_4$ was observed to be slightly higher than that of the modified electrode of NiO and Co_3O4. While the Co_3O4 electrode was observed to be inactive for methanol oxidation. Double step CA reveals that electrooxidation by $NiCo_2O_4$ is an irreversible reaction and diffusion-

controlled process. The linear relationship of oxidation peak current with methanol concentration and relatively low over-potential for the oxidation of methanol conclude that $NiCo_2O_4$ offers a promising catalyst for DMFC. [54]

Yingying Gu et al. [2015] synthesized Ni-Cr oxide nano-catalyst using thermal decomposition method and tested for methanol electrooxidation. Characterization was carried out by XRD and TEM. The results show that the rhombohedral structure of both NiO and Cr_2O_3 appears in the mixture at temperature 500-700°C, while the octahedral structure of $NiCr_2O_3$ was formed at 900°C. The electrocatalytic performance for methanol electro-oxidation was investigated by CV and CA in 0.25M NaOH and 1.0M methanol. Ni-Cr oxides prepared at lower temperatures show substantially higher electrocatalytic activity for methanol oxidation and stability in alkaline solution as compare to NiO nano-catalyst. The current density by Ni-Cr oxide electrode was $12.6mVcm^{-2}$. The synergistic effect between Ni and Cr oxides are responsible for the enhanced activity of Ni-Cr oxide nano-catalysts. Ni-Cr oxide catalyst can therefore be an effective and stable catalyst for methanol oxidation. [55]

Huazhen Cao et al. [2014] fabricated Ni catalyst on Cu modified TiO_2 nanorods substrate to study its electrochemical activity for methanol oxidation. Ordered TiO_2 nanorods were prepared by anodization followed by Cu deposition by using an electroless plating process. Ni nanoparticles were deposited on Cu deposited TiO_2 nanorods substrate by electrodeposition method. Ball flower shaped Ni particles and ball shaped Ni particles were formed on the supporting material by the two-step electrodeposition and one-step electrodeposition method. The ball flower shape of Ni particles increased the specific surface area of the working electrode. Ball flower-shaped $Ni/Cu/TiO_2$ anode showed current density $510mAcm^{-2}$ higher than ball flower-shaped Ni/ TiO_2 which is $202mAcm^{-2}$. The Cu in the interlayer increased electron conductivity which increases current density. [56]

Jie Yu, Yonghong Ni et al. [2018] synthesized Ni-NiO@C nanocomposite by using a one-step simple solution combustion technique using $NiCl_2$ as Ni source in ethanol

solvent. The nanocomposite was characterized by techniques XRD. XPS, EDS/SEM, HRTEM, and Raman. The surface area of Ni-NiO@C determined by BET analysis was higher than Ni-NiO and NiO. It means the existence of the carbon layer showed a dramatic increase in surface area and surface-active sites. Therefore Ni-NiO@C showed higher electrocatalytic activity for methanol electro-oxidation than Ni-NiO and NiO. Current densities at potential 0.7V for Ni-NiO@C/GCE, NiO/GCE, and Ni-NiO/GCE electrodes is 74mAcm^{-2}, 30 mAcm^{-2}, and 53 mAcm^{-2} respectively. Compared to other non-noble metals this catalyst can be conveniently prepared with greater activity and stability. [57]

Luoyuan Wang et al. [2016] synthesized NiO thin film by a simple anodization method. No conducting agent or binder was needed because the film was prepared directly on a metal substrate with higher adhesion strength. The film prepared was highly porous with higher mesopore volume, large surface area and showed rapid reaction kinetics as it facilitates the adsorption of reactant species on active sites. The current density for methanol oxidation by NiO thin film was 50mAcm^{-2} at a scan rate of 20mVs^{-1} in the presence of 1M methanol and 0.1M NaOH. Current density increased linearly with the increase in methanol concentration up to 2M methanol. This easy and low-cost anodization method is promising for fast electrode preparation for alkaline DMFCs.[58]

C.D. Gu et al. [2014] reported the synthesis of NiO electrodes by two different methods. NiO-DES was prepared by homogeneous precipitation in DES and NiO-AS was prepared by NaOH- induced aqueous-phase precipitation. Both NiO catalysts prepared by different methods have different structures and formation mechanism of final products. NiO-DES prepared by homogeneous precipitation in DES had more nucleation sites and produce a flower-like structure of NiO. In electrochemical studies, NiO-DES showed twice higher current density for methanol oxidation in 0.005M KOH and 0.1M methanol as compare to NiO-AS. NiO-DES electrode showed higher activity as it had higher stability, faster charge transfer, and better electrode accessibility. So, this method of homogeneous precipitation can be an efficient approach for homogeneous micro-structured electrocatalyst fabrication. [59]

Jinlan Xiao et al. [2017] reported multilayer NiO thin film fabricated on 3D nickel foam by simple electrochemical method at an optimal voltage and scan rate These parameters give rise to different film morphologies on nickel foam electrode thereby contributing to different efficiencies. Under optimum conditions, the electrocatalyst displayed higher activity as well as good stability. The NiO thin film displayed impressive electrocatalytic methanol oxidation current as 161.5mAcm^{-2} in 1M KOH and 0.3M methanol. Furthermore, NiO thin film also showed methanol-water electrolysis.[60]

G. Sonia Theres et al. [2018] reported the synthesis of Ni-Cu hybrid oxides deposited on ordered mesoporous carbon (OMC). By using reductant ($NaBH_4$) and capping agent (cetyltrimethylammonium bromides), pure Ni, Cu, and 15 weight% of different composition of Ni:Cu viz 1:1, 3:1, 1:3 were deposited on OMC. Of all the samples tested, NiCu hybrid oxides@OMC the electrocatalyst with Ni and Cu equal weight percent gives high surface area (436m^{2}g^{-1}), lowest onset potential (0.34V), maximum current density (182.07mAcm^{-2}), and R_{ct} value (0.355). Moreover, it retained 87.68 percent current density after 7200sec.[61]

Animesh Roy et al. [2019] reported copper oxide microstructure grown directly on substrate of nickel foam by electro-deposition method followed by annealing. For electrochemical methanol oxidation, CuO/Ni@400 electrocatalyst shows an onset potential of 0.38V vs Ag/AgCl which is lower than reported Cu electrocatalyst and an overpotential of 364mV for oxygen evolution. While current density observed by CuO/Ni@400 was 10mAcm^{-2} in an alkaline medium that is greater than the reported Cu electrocatalyst. The physio-chemical properties of the catalyst prepared were preserved by electrochemical methanol oxidation. The excellent catalytic efficiency of the CuO/Ni@400 catalyst is due to its special micro-structure. The easy manufacturing process and enhanced electrocatalytic efficiency suggest that CuO/Ni@400 can be a possible electrocatalyst for DMFCs in future.[62]

Inayat Ali Khan et al. [2006] synthesized graphic carbon encasing Cr_2O_3 nanoribbons which were used as supporting material for Ni-Pd catalyst. Ni-Pd was deposited on Cr_2O_3-

C support by sonication. Ni-Pd catalyst was characterized by some techniques PXRD, HR-TEM, EDX-SEM, BET, and it was found that integration of Ni-Pd lowered the surface area of supporting material from $438 m^2 g^{-1}$ to 171 $m^2 g^{-1}$. Ni-Pd electrocatalyst showed enhanced electrochemical catalytic efficiency for methanol oxidation and greater stability in acidic medium relative to others supported on glassy carbon and activated carbon.[63]

Chapter 3

3 Experimental Work

This chapter describes all experimental work performed in laboratory and presents effective synthesis method used for synthesis of desired materials. Basically, first part of this chapter explains catalyst synthesis and second part describes electrochemical assembly.

3.1 Synthesis of ceramic oxide thin films

Materials

All chemicals used were purchased from Sigma-Aldrich and used without any further processing. Chemicals used were nickel acetate tetrahydrate ($Ni(OAc)_2.4H_2O$), copper acetate anhydrous ($Cu(OAc)_2$), chromium acetylacetonate ($Cr(acac)_3$), magnesium acetate tetrahydrate ($Mg(OAc)_2.4H_2O$), methanol and ethanol.

Method of preparation

Thin-film deposition on FTO glass substrate was carried out at room temperature by using the dip-coating technique. Solutions for different electrodes were prepared by dissolving

their precursors in respective solvents and stirred continuously using a magnetic stirrer for 15 min at room temperature to form a homogenous mixture. Before deposition FTO glass slide was cut into 1cm × 2cm sizes and were cleaned thoroughly with detergent followed by washing in a 1:1 solution of ethanol and acetone in an ultrasonication bath for 20 min. Washed FTO glass substrates were dried in air at room temperature. Dried FTO glass substrate was immersed in precursor solution for 30 s. After coating, the film was dried on a hot plate at temperature 120 °C for 10 min. Finally, the film was formed by repeating this procedure four more times. The coated film was then calcined in a furnace at 500 °C for 3 h. For mixed metal oxide thin film deposition, the FTO substrate was dipped in two separate solutions of precursors turn by turn and repeat 5 more times.

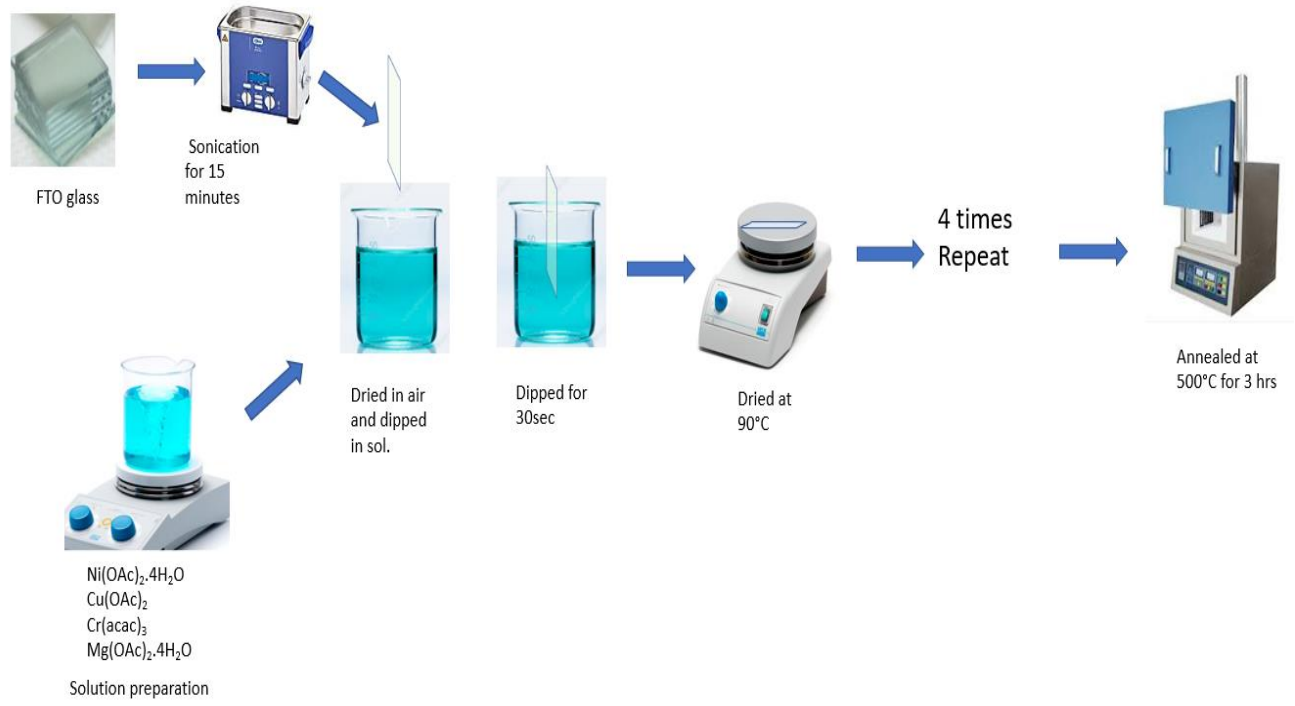

Figure 3.1 Schematic diagram of Synthesis of Metal Oxide Thin Films

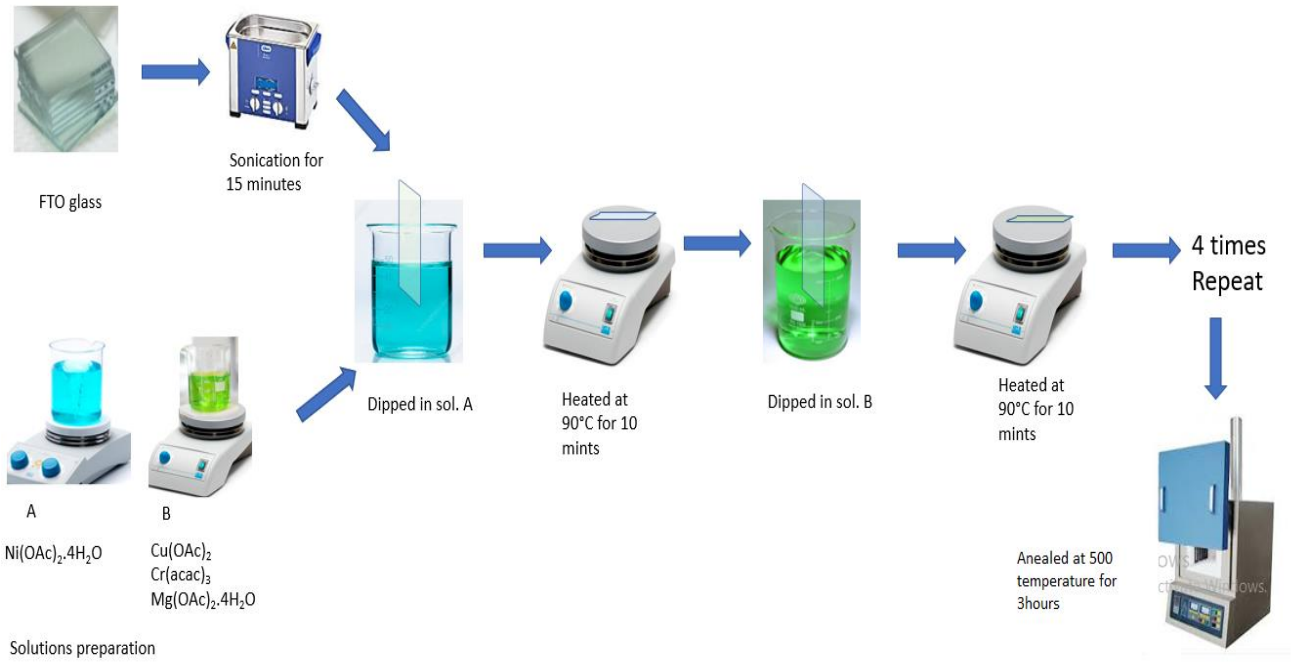

Figure 3.2 Schematic diagram of Synthesis of Mixed Metal Oxide Thin Films

Table 1 Ceramic Oxide Thin Films Synthesized

Sr. No.	**Thin Films**	**Precursor**	**Molarity(M)**	**Solvent**
1.	NiO	$Ni(OAc)_2.4H_2O$	0.1	Methanol
2.	CuO	$Cu(OAc)_2$	0.1	Ethanol
3.	NiO-CuO	$Ni(OAc)_2.4H_2O$ $Cu(OAc)_2$	0.1 0.1	Methanol Ethanol

Table 2 Ceramic Oxide Thin Films Synthesized

Sr. No.	**Thin Films**	**Precursor**	**Molarity(M)**	**Solvent**
1.	NiO	$Ni(OAc)_2.4H_2O$	0.1	Methanol
2.	Cr_2O_3	$Cr(acac)_3$	0.1	Ethanol
3.	Ni_{1-x} Cr_x O_2	$Ni(OAc)_2.4H_2O$ $Cr(acac)_3$	0.1 0.1	Methanol Ethanol

3.2 Characterization Instrumentations

The crystal structure of synthesized NiO, CuO, Cr_2O_3 thin films and their composites NiO-CuO, Ni_{1-x} Cr_x O_2 thin films were confirmed by X-Ray diffractometer (XRD STOE Germany) with Cu Kα radiation of λ=1.540608 Å and operated at 2θ (5° – 80°). The as prepared thin-films surface morphology and particle sizes were studied by Scanning Electron Microscopy (SEM VEG3 TESCAN). Furthermore, these synthesized thin films were investigated by Perkins spectrum 100 FT-IR spectrophotometer at wave number ranging from 4000 – 500cm^{-1}.

3.3 Experimental Assembly

GAMRY G750 in potentiostatic mode was used for conducting electrochemical studies. Electrocatalytic performance of synthesized thin-film catalysts for methanol oxidation was tested by linear sweep voltammetry (LSV), chronoamperometry (CA) and electrochemical impedance spectroscopy (EIS). All of the electrochemical measurements were performed by using a three-electrode setup containing Ag/AgCl serving as a

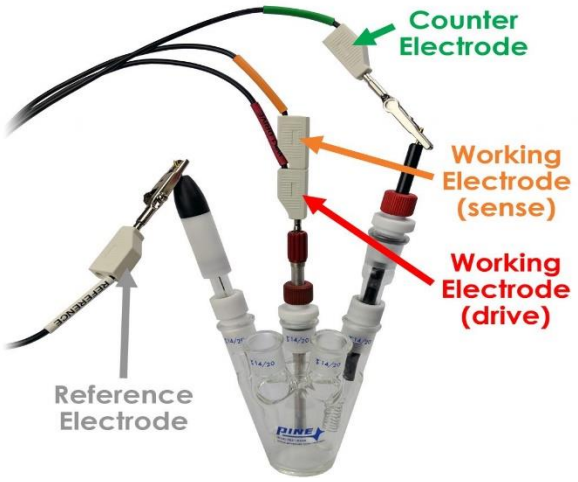

Figure 3.3 Three Electrode Electrochemical Cell

reference electrode, platinum wire as a counter electrode, and modified FTO as working electrode.

Figure 3.4 Potentiostate for Electrochemical Studies

Chapter 4

4 Result and Discussion

4.1 Characterizations

The samples synthesized were characterized for their structure, composition, and morphology studies by XRD and EDS-SEM. While electrocatalytic performance for methanol oxidation was tested by LSV, EIS, and CA analysis.

4.1.1 X-ray Diffraction (XRD)

XRD characterization was performed to determine the crystalline structure of synthesized thin films. Fig. 4.1 displays the XRD spectra of NiO, CuO, and NiO-CuO thin films after subtraction of FTO glass substrate peaks (JCPDS 00-001-0657). The XRD spectra of NiO displayed three diffraction peaks at $2\theta = 37.7°$, 43.3° and 61.6° indexed as (111), (200), and (220) plane orientations. All of these peak values perfectly resembles the cubic crystalline structure of NiO that corresponds very well to the JCPDS 01-073-1519 standard values. [64] In CuO XRD spectra two distinct diffraction peaks of almost equal intensities appeared at $2\theta = 35.4°$ and 38.6° assigned as (002) and (200) crystal planes. The diffraction peaks of CuO thin film are in complete agreement with standard monoclinic structure (JCPDS45-0937). [65] Crystallite sizes of NiO and CuO calculated using Debye-Scherrer equation is given below in Fig. 4.3. The XRD pattern of NiO-CuO thin film exhibits separate diffraction peaks of both NiO and CuO indexed to cubic phase of NiO (JCPDS 01-073-1519) and monoclinic phase of CuO (JCPDS45-0937). This

indicates that they are not forming a solid solution, and confirms the existence of crystalline NiO and CuO.

X-ray diffraction patterns of NiO, Cr_2O_3, and $Ni_{1-x}Cr_xO_2$ are shown in fig. 4.2. Diffraction peaks centered at 2θ = 24.5°, 33.6°, 36.3°, and 54.9° are characteristic peaks of Cr_2O_3 matched well with standard spectrum (JCPDS file 00-038-1479) not only in peak position but also in their relative intensities. It means the deposited Cr_2O_3 is rhombohedral in structure having (110), (113), (024), and (116) plane directions. [66] Crystallite sizes of synthesized Cr_2O_3 are given in fig. 4.3. In $Ni_{1-x}Cr_xO_2$ spectra, no distinct diffraction peak other than NiO peaks can be observed. While the high-intensity peak of NiO at 37.7° has shown a small shift toward a lower 2θ value when compared to NiO spectra. This shift is because of chromium ion occupation at the nickel site.

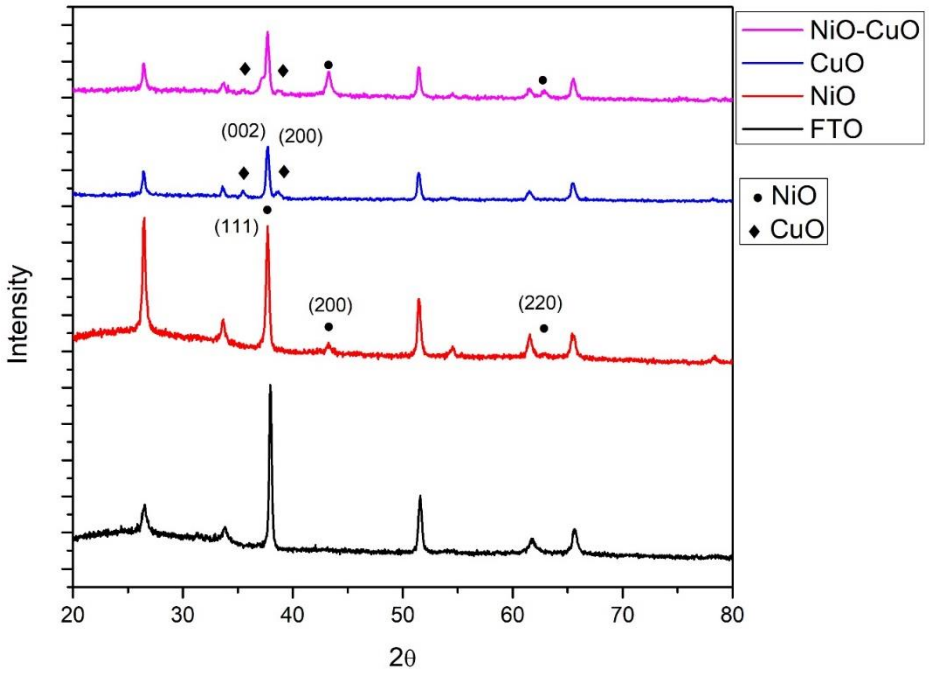

Figure 4.1 XRD Pattern of FTO, NiO, CuO, NiO-CuO Thin Films

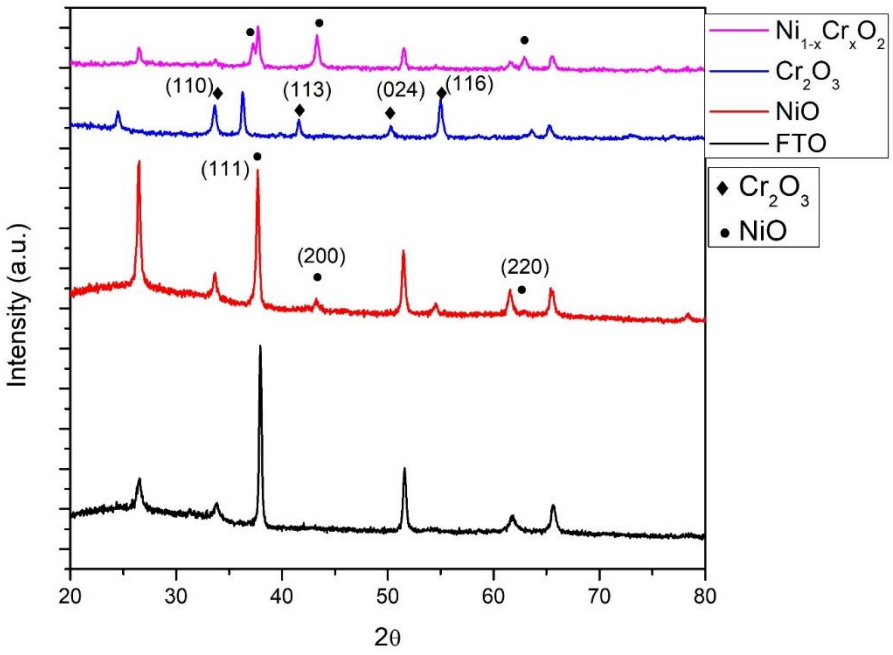

Figure 4.2 XRD Pattern of NiO, Cr_2O_3, $Ni_{1-x}Cr_xO_2$

Table 3 XRD Data of NiO, CuO and NiO-CuO Thin Films

Peak Position 2θ (°)	**Crystallite Size (nm)**	**hkl values**
NiO		
37.7	33	(111)
43.3	25.2	(200)
61.6	32.7	(220)
CuO		
35.4	22.1	(002)
38.6	22.3	(200)
NiO-CuO		
35.6	24.9	(002)
38.6	35.2	(200)
43.3	36.3	(200)

Table 4 XRD Data of Cr_2O_3 and $Ni_{1-x}Cr_xO_2$

Peak Position 2θ (°)	**Crystallite Size (nm)**	**hkl values**
Cr_2O_3		
24.5	34.5	(110)
33.6	35.5	(113)
36.3	44.4	(024)
54.9	38.0	(116)
$Ni_{1-x}Cr_xO_2$		
37.7	35.6	(111)
43.3	36.3	(200)
62.9	24.7	(220)

4.1.2 Fourier Transform Infrared Spectroscopy (FTIR)

FTIR spectra of NiO, CuO, NiO-CuO and Cr_2O_3, $Ni_{1-x}Cr_xO_2$ thin films are displayed in fig 4.6 and fig 4.7. In FTIR spectra no characteristic absorption band of metal oxides can be observed because they usually appear in range of 4000-500 cm^{-1}. While IR absorption band in each spectrum at 645 cm^{-1} is assigned to Sn-O bond vibration present in FTO glass substrate. It can be observed that these spectra do not exhibit any extra absorption band of impurity.

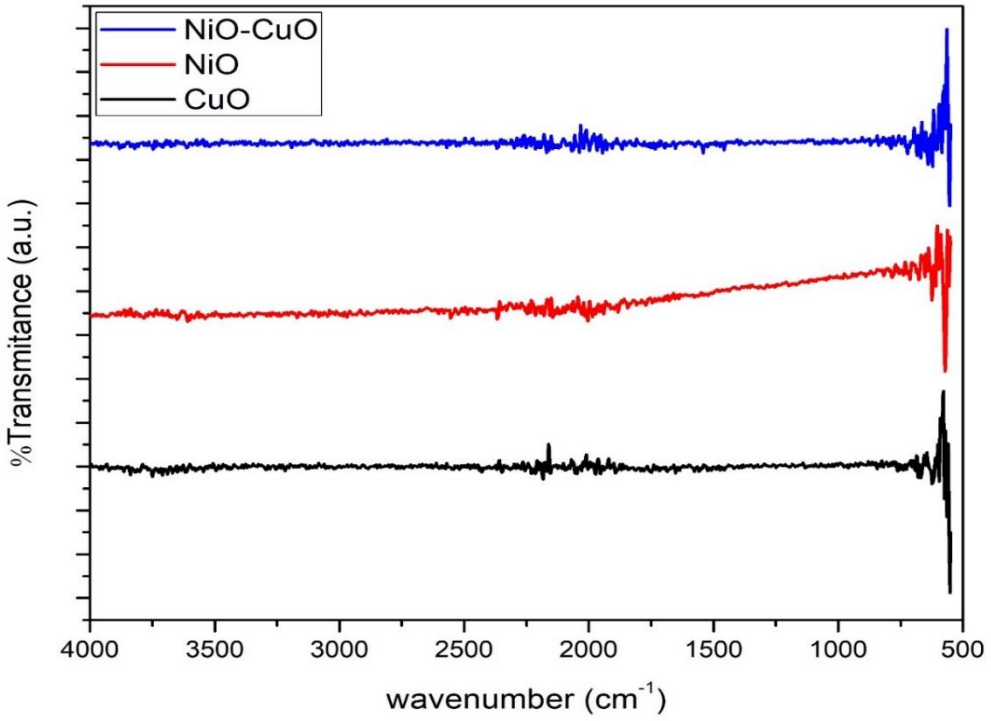

Figure 4.3 FTIR spectra of NiO, CuO, and NiO-CuO thin films

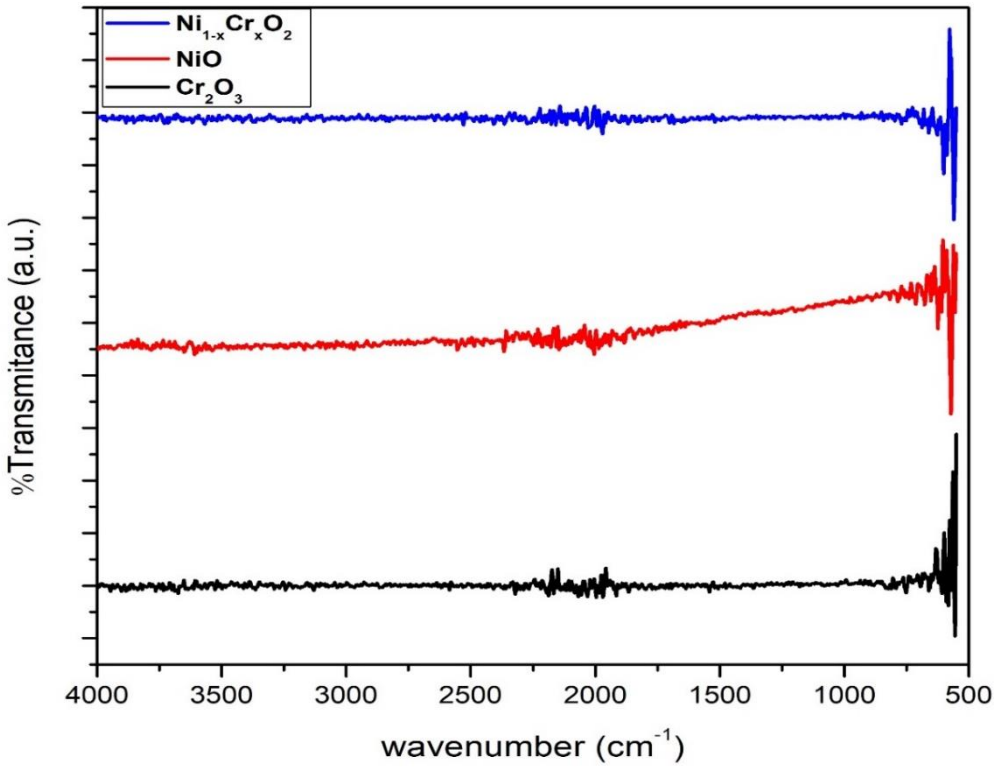

Figure 4.4 FTIR spectra of Cr_2O_3 and $Ni_{1-x}Cr_xO_2$ thin films

4.1.3 Scanning Electron Microscopy (SEM)

Scanning Electron Microscopy (SEM) is primarily used to verify the surface morphology of nanoparticles, particle size distribution, and whether or not they are agglomerated. Fig 4.4 displays SEM image of NiO, CuO, and NiO-CuO thin films. It is evident from the images that tiny grains are well interconnected and uniformly distributed. The average particle size of CuO and NiO-CuO was found to be 75nm and 150nm respectively. These tiny grains appear to be aggregated and have porosity around them. Fig 4.5 shows the surface morphology of Cr_2O_3 and $Ni_{1-x}Cr_xO_2$ thin films. Cr_2O_3 thin-film displays uniform deposition of irregular particles while porous morphology of $Ni_{1-x}Cr_xO_2$ thin film can be observed.

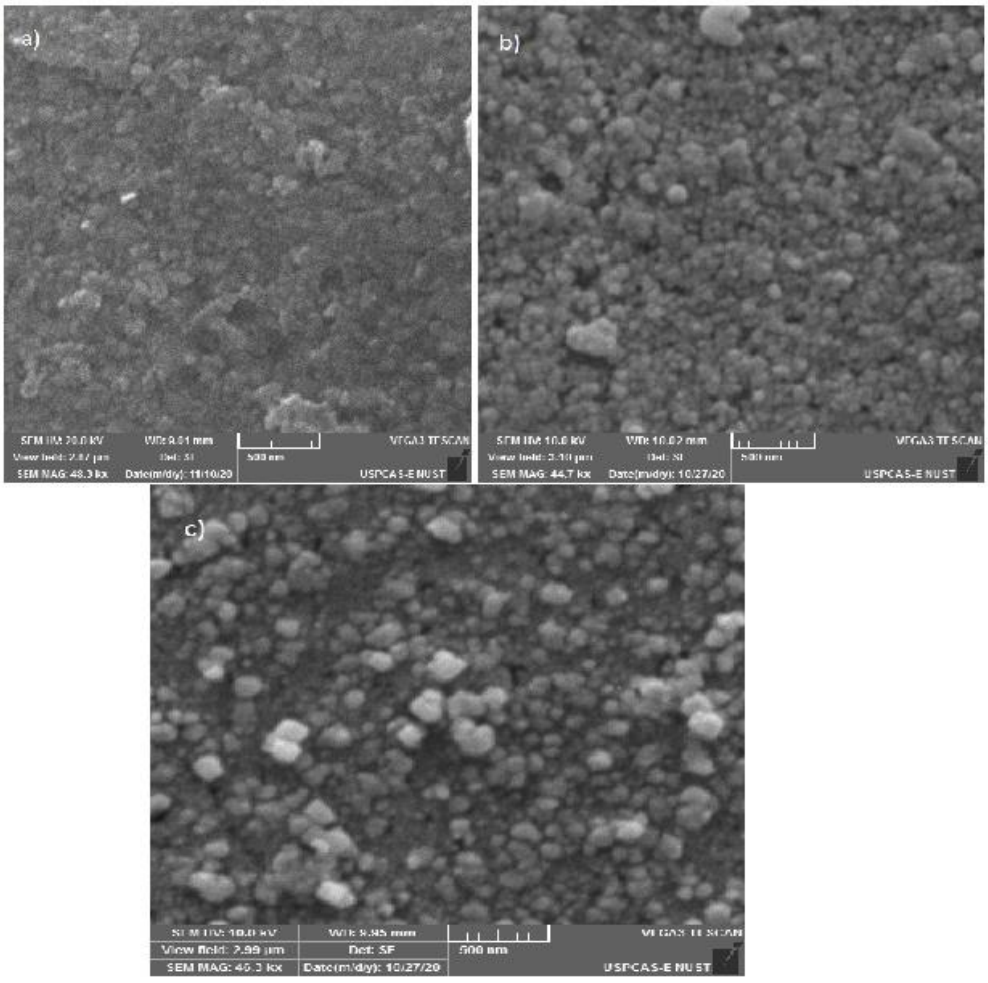

Figure 4.5 SEM images of **a)** NiO **b)** CuO **c)** NiO-CuO thin films

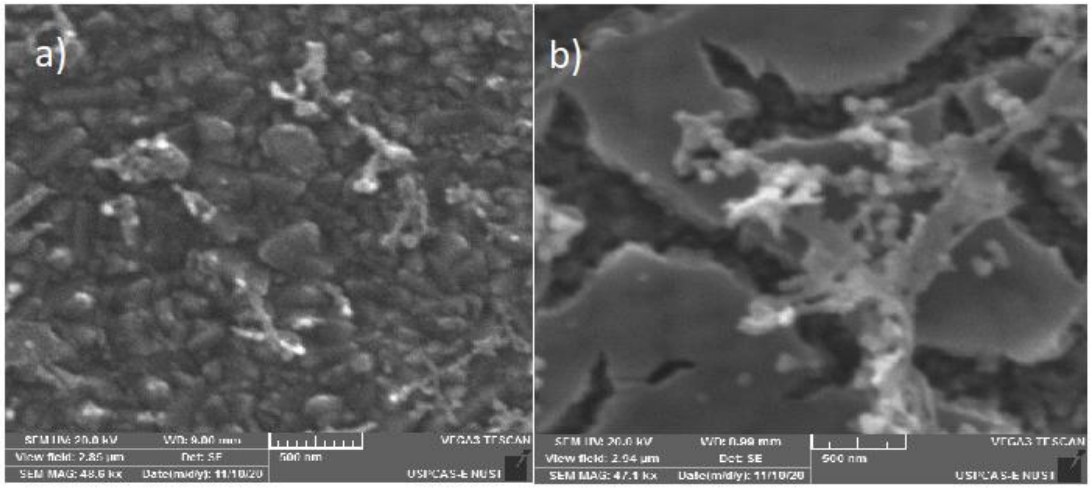

Figure 4.6 SEM images a) Cr_2O_3 b) $Ni_{1-x}Cr_xO_2$ thin films

4.1.4 Energy Dispersive X-Ray Spectroscopy (EDS)

EDS is an X-ray technique used to examine the elemental composition and distribution through element mapping. Fig 4.8 shows EDS spectra and atomic compositions of elements in the synthesized NiO, CuO, and NiO-CuO thin films. The data of this analysis confirms the presence of expected elements in as-synthesized thin films. The atomic ratio of Ni and Cu elements in NiO-CuO thin film is 1:1 as-synthesized. EDS spectra for Cr_2O_3 and $Ni_{1-x}Cr_xO_2$ are shown in Fig.4.9 EDS results of Cr_2O_3 thin film confirms presence of Cr and O elements. EDS results of $Ni_{1-x}Cr_xO_2$ thin film also confirms Cr doping in NiO lattice as atomic percentage of Cr to Ni is calculated to be 5%.

(a)

Element	Weight%	Atomic%
O K	39.69	75.56
Si K	10.35	11.23
Ni K	1.46	0.76
Sn L	48.50	12.45
Totals	100.00	

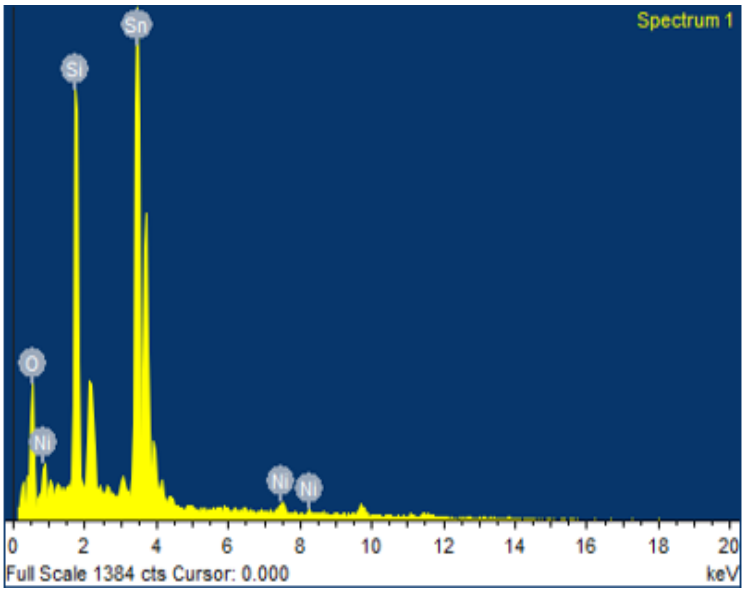

(b)

Element	Weight%	Atomic%
O K	33.04	74.76
Si K	4.43	5.70
Cu K	1.75	0.99
Sn L	60.79	18.54
Totals	100.00	

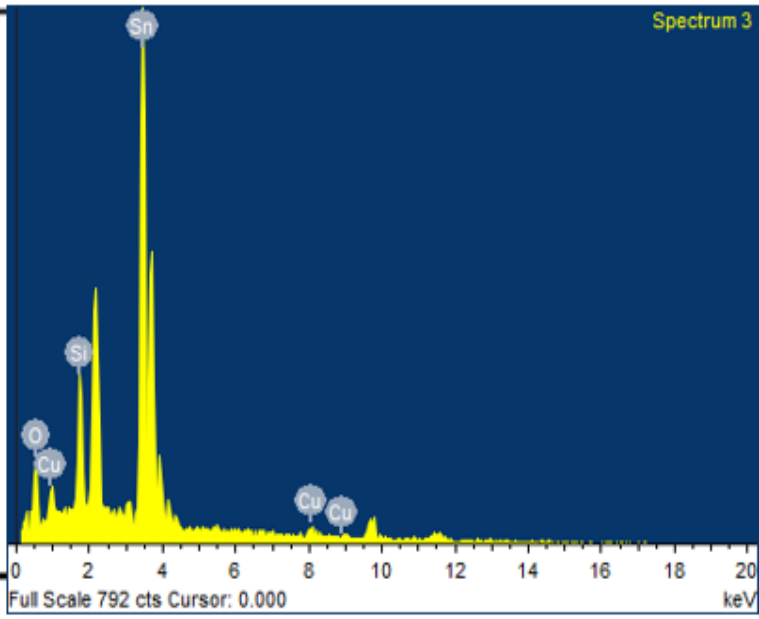

(a)

Element	Weight%	Atomic%
O K	39.44	79.59
Si K	4.44	5.10
Cr K	0.15	0.09
Sn L	55.97	15.22
Totals	100.00	

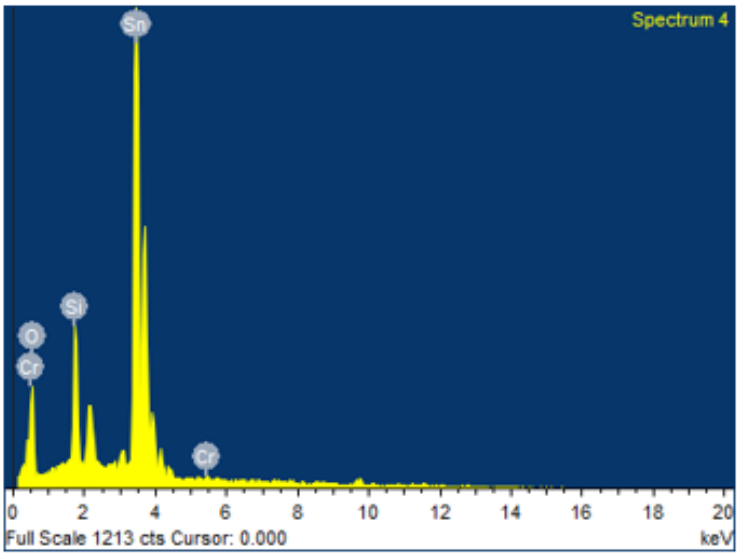

(b)

Element	Weight%	Atomic%
O K	44.46	82.26
Si K	2.58	2.71
Cr K	0.15	0.09
Ni K	6.94	3.50
Sn L	45.88	11.44

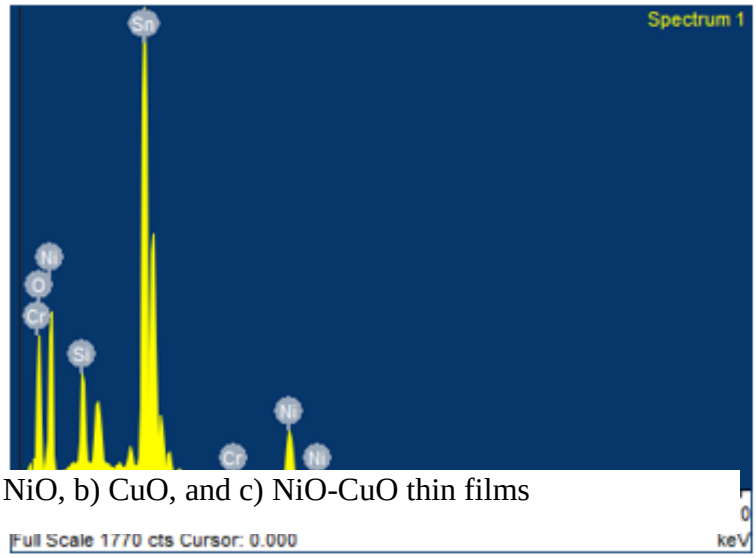

Figure 4.7 EDS results of a) NiO, b) CuO, and c) NiO-CuO thin films

Figure 4.8 EDS results of a) Cr_2O_3 b) $Ni_{1-x}\ Cr_x\ O_2$

4.1.5 Raman Spectroscopy

Raman spectra of NiO, CuO, and NiO-CuO thin films are shown in Fig 4.9. Raman spectrum of pure NiO thin film reveals two broad bands at 520 cm^{-1} and 1064 cm^{-1} which can be ascribed to NiO scattering of first order phonon (1P) and second order phonon (2P) respectively. Phonon is collective vibration of lattice atoms or molecules at a single frequency. [67] CuO shows two Raman active modes at 270 cm^{-1} and 603 cm^{-1} which can be allocated as A_g and B_g modes. A and B are 1-dimensional irreducible representations denoted when 1D vibration mode is symmetric or anti-symmetric with respect to rotation symmetric operation respectively. 'g' mode represents vibration mode symmetric with respect to center of inversion. [68] While NiO-CuO shows characteristic bands of both NiO and CuO confirming the presence of both metal oxides.

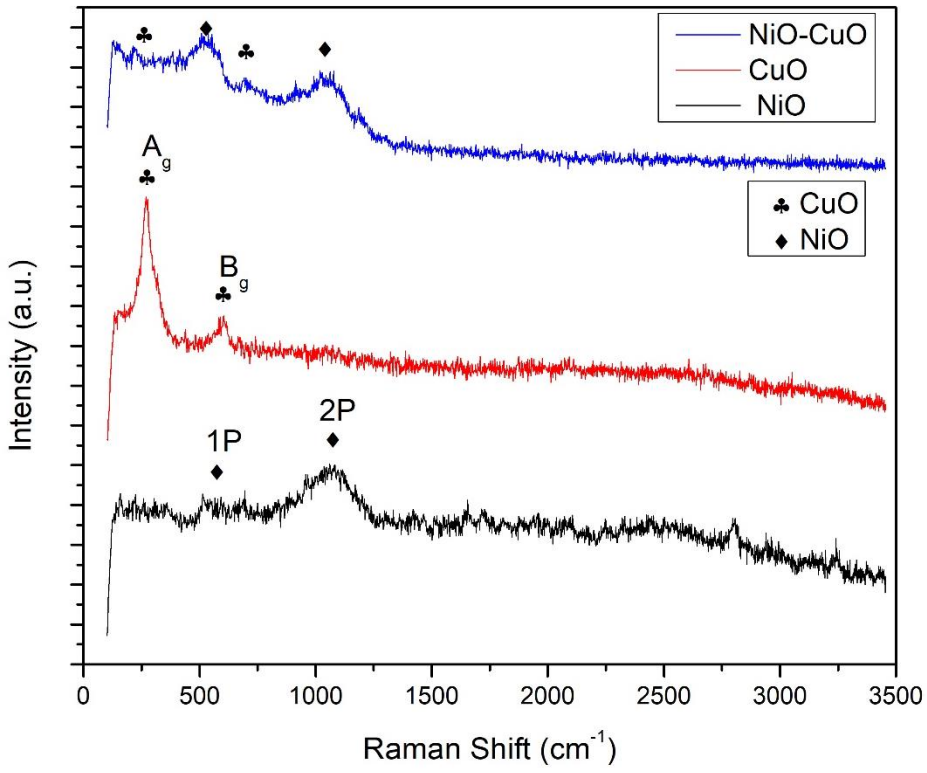

Figure 4.9 Raman Spectra of NiO, CuO, and NiO-CuO thin films

4.2 Electrochemical Studies

For electrochemical studies, GAMRY G750 was used in potentiostatic mode. For all electrochemical experiments, a three-electrode setup was used, using 0.5M NaOH as supporting electrolyte, modified FTO as working electrode, Ag/AgCl as a reference electrode and a platinum wire as a counter electrode.

4.2.1 Linear Sweep Voltammetry (LSV)

Fig 4.10. displays LSV curves of NiO, CuO, and NiO-CuO thin films at various methanol concentrations in 0.5 M NaOH recorded at a scan rate of 50 mVs^{-1}. The current density of NiO, CuO, and NiO-CuO thin films increased on the addition of methanol as compared to that in the absence of methanol. The increase in current density was observed by increasing methanol concentration from 0 M to 0.3 M. At potential 0.6 V current densities of NiO, CuO, and NiO-CuO thin films are 4.2 $mAcm^{-2}$, 2 $mA0.5cm^{-2}$, and 6.1 $mA0.5cm^{-2}$ in the presence of 0.3 M methanol respectively. In order to determine effectiveness of electrocatalysts for methanol oxidation onset potential is an important parameter as this is the point where reaction product is formed. There is a strong change in onset potential before and after addition of methanol. The onset potential of catalysts for methanol electro-oxidation shifted from 0.8 V to 0.43 V on the addition of methanol. All catalysts exhibit catalytic activity for methanol oxidation while the activity of pure NiO and pure CuO thin film is lower than NiO-CuO thin film as shown in fig 4.10d). The enhancement of methanol oxidation at NiO-CuO catalyst can be attributed to the synergistic role of both metal oxides.

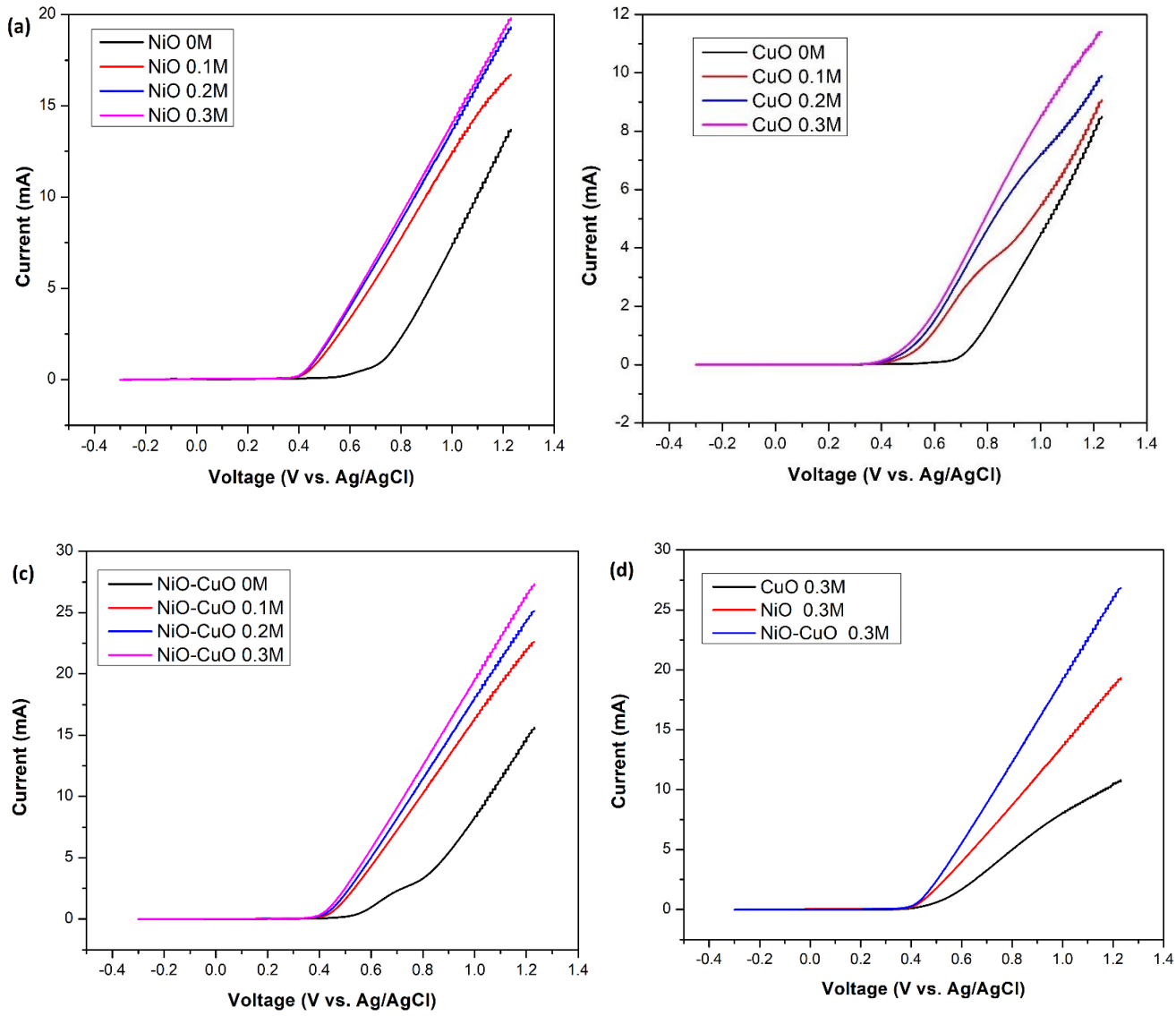

Figure 4.10 Linear Sweep Voltammetry of a) NiO b) CuO c) NiO-CuO thin films at 0M, 0.1M, 0.2M, 0.3M methanol concentration d) Comparison of NiO, CuO, NiO-CuO thin films at 0.3M methanol concentration at 50mVs^{-1}.

LSV results of Cr_2O_3 and Ni_{1-x} Cr_x O_2 thin films at different methanol concentrations in 0.5 M NaOH were recorded at a scan rate of 50 mVs^{-1}. Cr_2O_3 thin film is the poorest catalyst of all samples for methanol oxidation. The onset potential of Ni_{1-x} Cr_x O_2 thin film decreased to 0.4 V on addition of methanol which means methanol oxidation reaction

started at that potential. The current density of Ni_{1-x} Cr_x O_2 thin film is 6.5mA/cm vs. 0.6 V in the presence of 0.3 M methanol. The catalytic activity of Ni_{1-x} Cr_x O_2 thin film is significantly larger than the catalytic activity of pure NiO thin film. The synergistic effect between Ni and Cr oxide is responsible for the enhanced activity of Ni_{1-x} Cr_x O_2 thin film.

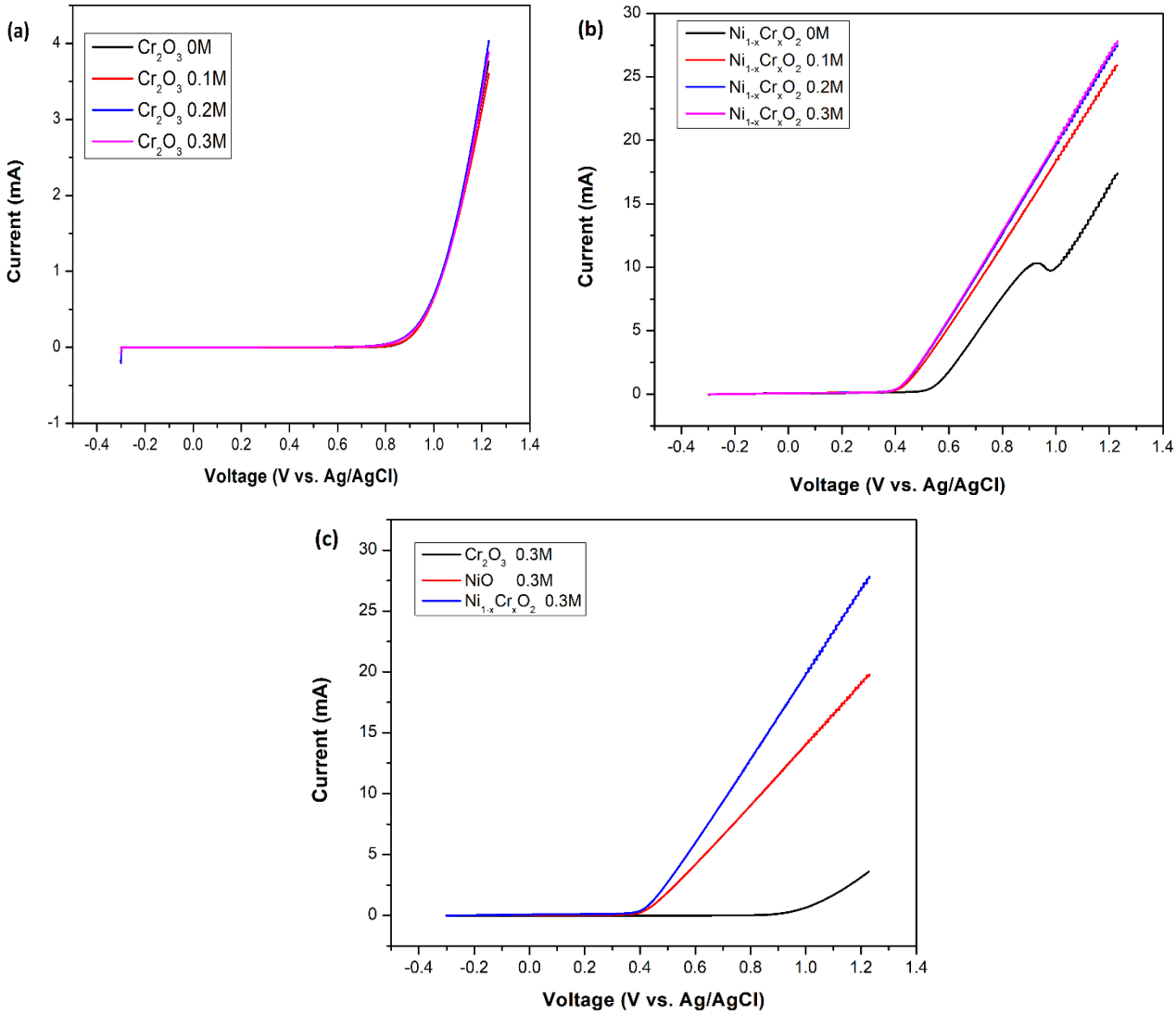

Figure 4.11 Linear Sweep Voltammetry of a) Cr_2O_3 b) Ni_{1-x} Cr_x O_2 thin films at 0M, 0.1M, 0.2M, 0.3M methanol concentration d) Comparison of Cr_2O_3 and Ni_{1-x} Cr_x O_2 at 0.3M methanol concentration

4.2.2 Electrochemical Impedance Spectroscopy (EIS)

EIS test was performed to further analyze the electro-catalytic activity of the catalysts studied for methanol oxidation. EIS results are also dependent on methanol concentration.Fig.4.13 displays Nyquist plot of NiO-CuO thin film in 0.5 M NaOH before and after addition of 0.3 M methanol. Figure 4.12 shows the EIS plot of $Ni_{1-x}Cr_xO_2$ thin film in 0.5 M NaOH before and after addition of 0.3 M methanol. The Nyquist plot displays two semicircles one in the high frequency region related to solution resistance and the second in the low frequency region related to charge transfer resistance (R_{ct}). R_{ct} indicates the rate of charge exchange at electrochemical interface between aqueous solution and composite ions of electrolyte. In both EIS plots, a smaller diameter of the second semicircle can be observed after the addition of methanol which suggests fast electron-charge transfer. After addition of methanol, the value of R_{ct} calculated for NiO-CuO and $Ni1_xCr_xO_2$ thin film is 3.18 Ω/cm^2 and 2.85 Ωcm^{-2} respectively. These small R_{ct} values in methanol indicate low charge transfer resistance, improved conductivity, and higher catalytic activity for NiO-CuO and $Ni1_xCr_xO_2$ electrocatalysts.

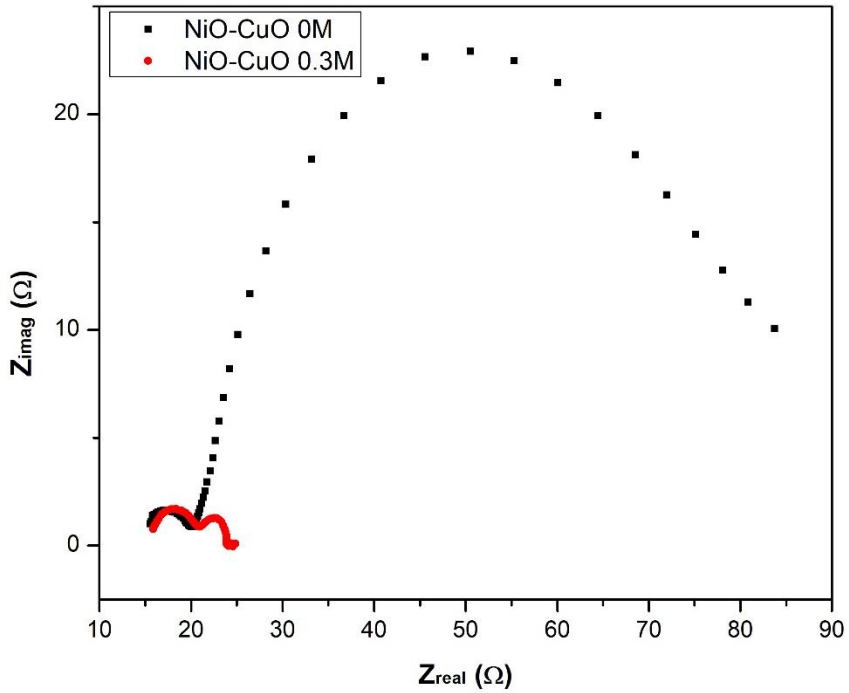

Figure 4.13 EIS plot of NiO-CuO thin film in 0.5M NaOH before and after addition of 0.3M methanol

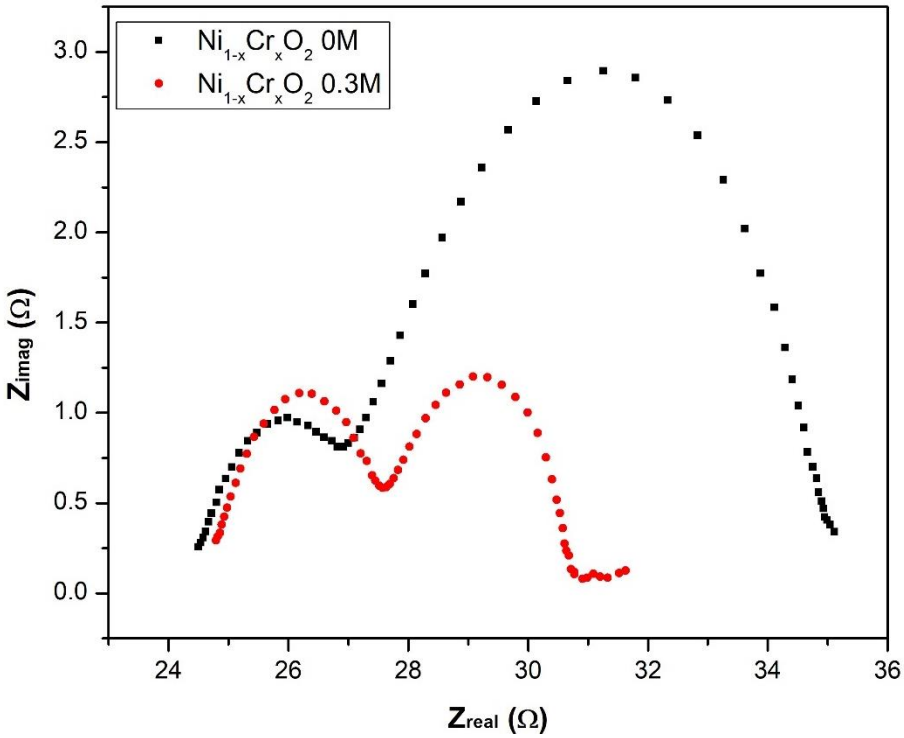

Figure 4.12 EIS plot of $Ni_{1-x}Cr_xO_2$ thin film in 0.5 M NaOH before and after addition of 0.3 M methanol

4.2.3 Chronoamperometry (CA)

Chronoamperometric test was carried out to characterize the stability for methanol oxidation reaction on NiO-CuO and $Ni_{1x}\,Cr_x\,O_2$ thin films in 0.5 M NaOH and 0.3 M methanol. It is obvious that in first few seconds before relative steady state was reached, both samples displayed some current decay. This decay can be due to the adsorption of reaction intermediates like CO. Furthermore, this decrease in current density can be due to decrease in methanol concentration near electrode surface by rapid oxidation of methanol at start. Subsequently these changes are under mass transfer control process. NiO-CuO and $Ni_{1x}\,Cr_x\,O_2$ thin films have shown stability of 95% and 89% at potential of 0.6 V for 2000 s. Moreover, NiO-CuO and $Ni_{1x}\,Cr_x\,O_2$ electrodes have maintained catalytic activity and stability toward methanol oxidation for long time.

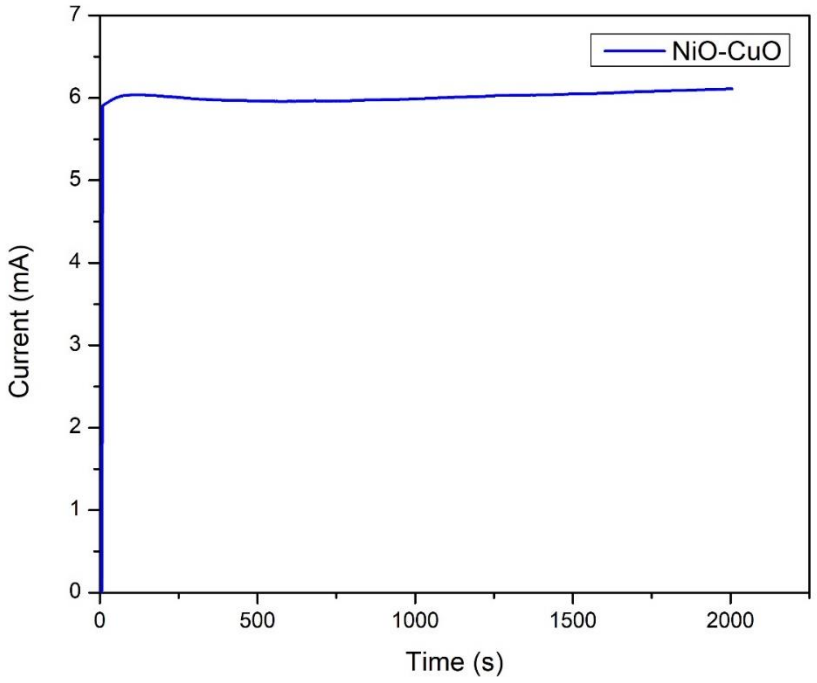

Figure 4.14 Chronoamperometric graph of NiO-CuO in 0.5M NaOH and 0.3M methanol

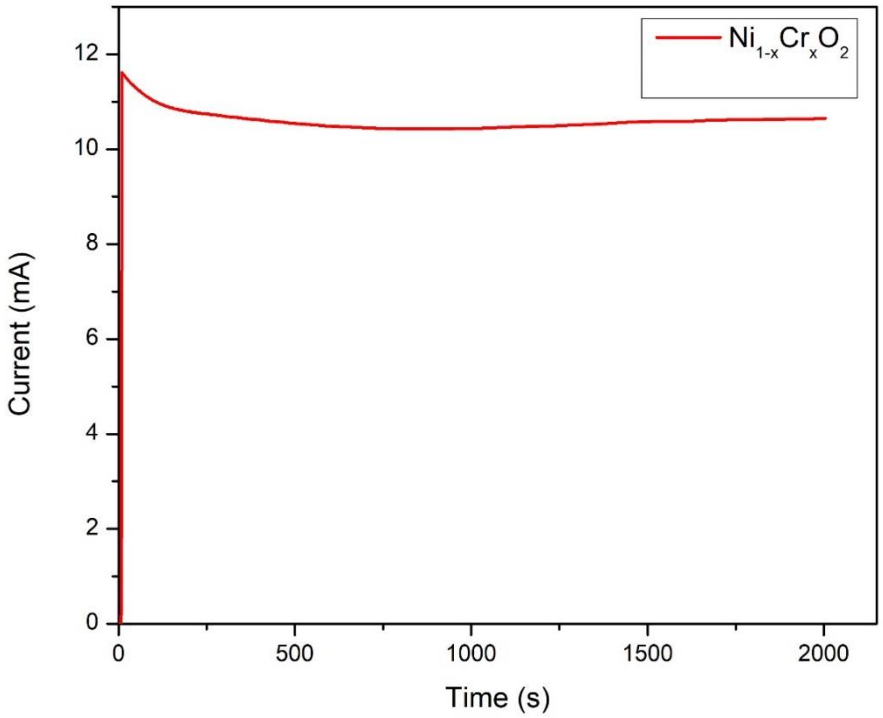

Figure 4.15 Chronoamperometric graph of $Ni_{1x}Cr_xO_2$ in 0.5 M NaOH and 0.3 M methanol

Chapter 5

5 Conclusion

5.1 Summary

NiO, CuO, Cr_2O_3, NiO-CuO, and $Ni_{1-x}Cr_xO_2$ thin films were synthesized by a simple dip-coating method. The precursors used were $Ni(OAc)_2.4H_2O$, $Cu(OAc)_2$, and $Cr(acac)_3$ that are easily soluble in volatile organic solvents like methanol and ethanol. Surface morphology, phase structure, and chemical composition of prepared samples were analyzed by techniques scanning electron microscopy (SEM), energy dispersive spectroscopy (EDS), Raman, and FTIR. The electrochemical behavior of prepared catalysts for methanol oxidation was investigated by several techniques including linear sweep voltammetry (LSV), electrochemical impedance spectroscopy (EIS), and chronoamperometry (CA) using three-electrode system i.e., modified FTO as working electrode, Ag/AgCl as a reference electrode, and Pt as a counter electrode. Current densities of NiO-CuO and $Ni_{1-x}Cr_xO_2$ thin films are 6.1 mA0.5cm^{-2} and 6.5 $mAcm^{-2}$ vs. 0.6 V in the presence of 0.3 M methanol. The increase in the catalytic activity of NiO-CuO and $Ni_{1-x}Cr_xO_2$ thin films can be due to a synergistic effect between metal oxides. The findings of EIS and CA also support the above results and help to explain the assumptions described. All the results of NiO-CuO and $Ni_{1-x}Cr_xO_2$ thin films showed better electrocatalytic activity, lower charge transfer resistance, good stability, and resistant to poisoning effect as compare to pure NiO, CuO, and Cr_2O_3 thin films. These catalysts are less expensive and can be a good candidate for the direct methanol fuel cell.

5.2 Future Recommendations

- These oxides based ceramic thin films can be tested for photo-electrochemical oxidation of methanol in future.
- Ceramic oxide thin films can be checked for sensing application.
- These catalysts can also be tested for electrochemical water splitting.

References

1. Wang, P., et al., *Well-dispersed NiO nanoparticles supported on nitrogen-doped carbon nanotube for methanol electrocatalytic oxidation in alkaline media.* 2017. **392**: p. 562-571.
2. Rafique, M.M., S.J.R. Rehman, and S.E. Reviews, *National energy scenario of Pakistan–Current status, future alternatives, and institutional infrastructure: An overview.* 2017. **69**: p. 156-167.
3. O'hayre, R., et al., *Fuel cell fundamentals*. 2016: John Wiley & Sons.
4. Carrette, L., K.A. Friedrich, and U.J.C. Stimming, *Fuel cells: principles, types, fuels, and applications.* 2000. **1**(4): p. 162-193.
5. Blomen, L.J. and M.N. Mugerwa, *Fuel cell systems*. 2013: Springer Science & Business Media.
6. Vielstich, W., A. Lamm, and H.A. Gasteiger, *Handbook of fuel cells: fundamentals technology and applications*. Vol. 2. 2003: Wiley New York.
7. Coutanceau, C., et al., *Development of electrocatalysts for solid alkaline fuel cell (SAFC).* 2006. **156**(1): p. 14-19.
8. Wang, Y., et al., *A review of polymer electrolyte membrane fuel cells: Technology, applications, and needs on fundamental research.* 2011. **88**(4): p. 981-1007.
9. Gamburzev, S. and A.J.J.J.o.p.s. Appleby, *Recent progress in performance improvement of the proton exchange membrane fuel cell (PEMFC).* 2002. **107**(1): p. 5-12.

10. Vaghari, H., et al., *Recent advances in application of chitosan in fuel cells.* 2013. **1**(1): p. 16.
11. Sammes, N., et al., *Phosphoric acid fuel cells: Fundamentals and applications.* 2004. **8**(5): p. 372-378.
12. Lu, Y., et al., *Solid oxide fuel cell technology for sustainable development in China: An over-view.* 2018. **43**(28): p. 12870-12891.
13. Singhal, S.C.J.S.s.i., *Advances in solid oxide fuel cell technology.* 2000. **135**(1-4): p. 305-313.
14. Kim, B.H., et al., *Challenges in microbial fuel cell development and operation.* 2007. **76**(3): p. 485.
15. Liu, H., et al., *A review of anode catalysis in the direct methanol fuel cell.* 2006. **155**(2): p. 95-110.
16. Hou, G.-Y., et al., *Electrocatalytic performance of Ni-Ti-O nanotube arrays/NiTi alloy electrode annealed under H2 atmosphere for electro-oxidation of methanol.* 2016. **41**(22): p. 9295-9302.
17. Rahim, M.A., R.A. Hameed, and M.J.J.o.p.s. Khalil, *The role of a bimetallic catalyst in enhancing the electro-catalytic activity towards methanol oxidation.* 2004. **135**(1-2): p. 42-51.
18. Wilberforce, T., et al., *Advances in stationary and portable fuel cell applications.* 2016. **41**(37): p. 16509-16522.
19. Kamarudin, S.K., F. Achmad, and W.R.W.J.I.J.o.h.e. Daud, *Overview on the application of direct methanol fuel cell (DMFC) for portable electronic devices.* 2009. **34**(16): p. 6902-6916.
20. Li, X. and A.J.J.o.P.S. Faghri, *Review and advances of direct methanol fuel cells (DMFCs) part I: Design, fabrication, and testing with high concentration methanol solutions.* 2013. **226**: p. 223-240.
21. Arico, A., S. Srinivasan, and V.J.F.c. Antonucci, *DMFCs: from fundamental aspects to technology development.* 2001. **1**(2): p. 133-161.

22. Carter, C.B. and M.G. Norton, *Ceramic materials: science and engineering*. Vol. 716. 2007: Springer.
23. Chen, F.P., *Ceramic material and method of making the same*. 1961, Google Patents.
24. Keane, M.J.J.o.m.s., *Ceramics for catalysis.* 2003. **38**(23): p. 4661-4675.
25. Trasatti, S.J.E.a., *Physical electrochemistry of ceramic oxides.* 1991. **36**(2): p. 225-241.
26. Sayer, M. and K.J.S. Sreenivas, *Ceramic thin films: fabrication and applications.* 1990. **247**(4946): p. 1056-1060.
27. Abegunde, O.O., et al., *Overview of thin film deposition techniques.* 2019. **6**(2): p. 174-199.
28. Kawazoe, H., et al., *Oxide thin film*. 2001, Google Patents.
29. Nix, W.D.J.M.t.A., *Mechanical properties of thin films.* 1989. **20**(11): p. 2217.
30. Haukka, S.P., et al., *Thin films*. 2008, Google Patents.
31. Teixeira, V., et al., *High barrier plastics using nanoscale inorganic films*, in *Multifunctional and nanoreinforced polymers for food packaging*. 2011, Elsevier. p. 285-315.
32. Scriven, L.J.M.O.P.L.A., *Physics and applications of dip coating and spin coating.* 1988. **121**.
33. Brinker, C.J., *Dip coating*, in *Chemical Solution Deposition of Functional Oxide Thin Films*. 2013, Springer. p. 233-261.
34. Brinker, C., et al., *Fundamentals of sol-gel dip coating.* 1991. **201**(1): p. 97-108.
35. Takahashi, Y., et al., *Dip-coating of ITO films.* 1997. **218**: p. 129-134.
36. Warren, B.E., *X-ray Diffraction*. 1990: Courier Corporation.
37. Azároff, L.V., et al., *X-ray Diffraction*. Vol. 3. 1974: McGraw-Hill New York.
38. Zhou, W., et al., *Fundamentals of scanning electron microscopy (SEM)*, in *Scanning microscopy for nanotechnology*. 2006, Springer. p. 1-40.
39. Inkson, B., *Scanning electron microscopy (SEM) and transmission electron microscopy (TEM) for materials*

characterization, in *Materials characterization using nondestructive evaluation (NDE) methods*. 2016, Elsevier. p. 17-43.
40. Schmitt, J., H.-C.J.I.B. Flemming, and Biodegradation, *FTIR-spectroscopy in microbial and material analysis.* 1998. **41**(1): p. 1-11.
41. Kissinger, P.T. and W.R.J.J.o.C.E. Heineman, *Cyclic voltammetry.* 1983. **60**(9): p. 702.
42. Mabbott, G.A.J.J.o.C.e., *An introduction to cyclic voltammetry.* 1983. **60**(9): p. 697.
43. Evans, D.H., et al., *Cyclic voltammetry*. 1983, ACS Publications.
44. Molina, A., C. Serna, and J.n.J.J.o.E.C. González, *General analytical solution for a catalytic mechanism in potential step techniques at hemispherical microelectrodes: Applications to chronoamperometry, cyclic staircase voltammetry and cyclic linear sweep voltammetry.* 1998. **454**(1-2): p. 15-31.
45. Yan, Q., *Synthesis, characterization and catalytic studies of carbon-based nano materials*. 2011, Mississippi State University.
46. Lasia, A., *Electrochemical impedance spectroscopy and its applications*, in *Modern aspects of electrochemistry*. 2002, Springer. p. 143-248.
47. Danaee, I., et al., *Electrooxidation of methanol on NiMn alloy modified graphite electrode.* 2010. **55**(6): p. 2093-2100.
48. Hu, Y., et al., *Synthesis of graphene-supported hollow Pt–Ni nanocatalysts for highly active electrocatalysis toward the methanol oxidation reaction.* 2012. **85**: p. 314-321.
49. Sun, S. and Z.J.J.E.A. Xu, *Composition dependence of methanol oxidation activity in nickel–cobalt hydroxides and oxides: an optimization toward highly active electrodes.* 2015. **165**: p. 56-66.
50. Hassan, H. and R.H.J.S.S.I. Tammam, *Preparation of Ni-metal oxide nanocomposites and their role in enhancing the*

electro-catalytic activity towards methanol and ethanol. 2018. **320**: p. 325-338.
51. Danaee, I., et al., *Electrocatalytic oxidation of methanol on Ni and NiCu alloy modified glassy carbon electrode.* 2008. **33**(16): p. 4367-4376.
52. Tammam, R., A. Fekry, and M.J.i.j.o.h.e. Saleh, *Electrocatalytic oxidation of methanol on ordered binary catalyst of manganese and nickel oxide nanoparticles.* 2015. **40**(1): p. 275-283.
53. Hassan, H., Z.A. Hamid, and R.M.J.C.J.o.C. El-Sherif, *Electrooxidation of methanol and ethanol on carbon electrodeposited Ni–MgO nanocomposite.* 2016. **37**(4): p. 616-627.
54. Prathap, M.A. and R.J.N.E. Srivastava, *Synthesis of NiCo2O4 and its application in the electrocatalytic oxidation of methanol.* 2013. **2**(5): p. 1046-1053.
55. Gu, Y., et al., *Synthesis of bimetallic Ni–Cr nano-oxides as catalysts for methanol oxidation in NaOH solution.* 2015. **15**(5): p. 3743-3749.
56. Cao, H., et al., *Ball-flower-shaped Ni nanoparticles on Cu modified TiO2 nanotube arrays for electrocatalytic oxidation of methanol.* 2014. **125**: p. 275-281.
57. Yu, J., et al., *Simple solution-combustion synthesis of Ni-NiO@ C nanocomposites with highly electrocatalytic activity for methanol oxidation.* 2018. **112**: p. 119-126.
58. Wang, L., et al., *Facile synthesis of a mechanically robust and highly porous NiO film with excellent electrocatalytic activity towards methanol oxidation.* 2016. **8**(21): p. 11256-11263.
59. Gu, C., et al., *NiO electrode for methanol electro-oxidation: Mesoporous vs. nanoparticulate.* 2014. **39**(21): p. 10892-10901.
60. Xiao, J., et al., *Electrochemical formation of multilayered NiO film/Ni foam as a high-efficient anode for methanol electrolysis.* 2017. **21**(8): p. 2301-2311.

61. Theres, G.S., et al., *Synergistic impact of Ni–Cu hybrid oxides deposited on ordered mesoporous carbon scaffolds as non-noble catalyst for methanol oxidation.* 2019. **54**(2): p. 1502-1519.
62. Roy, A., et al., *Electrochemical deposition of self-supported bifunctional copper oxide electrocatalyst for methanol oxidation and oxygen evolution reaction.* 2019. **76**: p. 515-523.
63. Khan, I.A., et al., *Cr2O3–carbon composite as a new support material for efficient methanol electrooxidation.* 2016. **77**: p. 221-227.
64. Ghalmi, Y., et al., *Capacitance performance of NiO thin films synthesized by direct and pulse potentiostatic methods.* 2019. **25**(12): p. 6025-6033.
65. Akgul, F.A., et al., *Influence of thermal annealing on microstructural, morphological, optical properties and surface electronic structure of copper oxide thin films.* 2014. **147**(3): p. 987-995.
66. Al-Saadi, T.M. and N.A.J.S. Hameed, *Synthesis and structural characterization of Cr2O3 nanoparticles prepared by using Cr (NO3) 3. 9H2O and triethanolamine under microwave irradiation.* 2015. **44**.
67. Qiu, Z., et al., *High performance asymmetric supercapacitors with ultrahigh energy density based on hierarchical carbon nanotubes@ NiO core–shell nanosheets and defect-introduced graphene sheets with hole structure.* 2017. **7**(13): p. 7843-7856.
68. Guha, S., D. Peebles, and J.T.J.B.o.M.S. Wieting, *Raman and infrared studies of cupric oxide.* 1991. **14**(3): p. 539-543.